frontiers in Earth Science

ORIGINAL RESEARCH
published: 29 March 2022
doi: 10.3389/feart.2022.845763

Petrogenesis and Geodynamic Implications of Late Triassic Mogetong Adakitic Pluton in East Kunlun Orogen, Northern Tibet: Constraints from Zircon U–Pb–Hf Isotopes and Whole-Rock Geochemistry

Jie Gan[1,2]*, Fuhao Xiong*[1,2,3]**, Qianru Xiao*[1,4]**, Wei Wang*[2] *and Dongdong Yan*[2]

[1]*Key Laboratory of Tectonic Controls on Mineralization and Hydrocarbon Accumulation, Chengdu University of Technology, Chengdu, China,* [2]*College of Earth Science, Chengdu University of Technology, Chengdu, China,* [3]*State Key Laboratory of Oil and Gas Reservoir Geology and Exploitation, Chengdu University of Technology, Chengdu, China,* [4]*College of Tourism and Urban-Rural Planning, Chengdu University of Technology, Chengdu, China*

OPEN ACCESS

Edited by:
Guillermo Booth-Rea, University of Granada, Spain

Reviewed by:
Liang Liu, Institute of Geochemistry (CAS), China
Bin Liu, Yangtze University, China

****Correspondence:***
Fuhao Xiong
xiongfuhao2014@cdut.edu.cn
Qianru Xiao
xiaoqianru@cdut.edu.cn

Specialty section:
This article was submitted to "Structural Geology and Tectonics", a section of the journal Frontiers in Earth Science

Received: *30 December 2021*
Accepted: *31 January 2022*
Published: *29 March 2022*

Citation:
Gan J, Xiong F, Xiao Q, Wang W and Yan D (2022) Petrogenesis and Geodynamic Implications of Late Triassic Mogetong Adakitic Pluton in East Kunlun Orogen, Northern Tibet: Constraints from Zircon U–Pb–Hf Isotopes and Whole-Rock Geochemistry. Front. Earth Sci. 10:845763. doi: 10.3389/feart.2022.845763

Adakites or adakitic rocks usually show special geochemical signatures and are petrological probes to reveal the tectono–magmatic evolutionary history of paleo–orogenic belts. Here, we present a comprehensive study on the zircon U–Pb geochronology, whole-rock geochemistry, and zircon Lu-Hf isotopes of Mogetong adakitic pluton in East Kunlun orogen, Northern Tibetan Plateau, to constrain its petrogenesis and tectonic setting, and thus to reveal its implications for the Paleo–Tethyan orogeny. The studied pluton comprises of quartz monzonite porphyry with zircon U–Pb crystallization age of ca. 215 Ma, which is coeval to their diorite enclaves (ca. 212 Ma). The quartz monzonite porphyries have intermediate SiO_2 (63.31–65.74 wt %), relatively high Al_2O_3 (15.52–16.02 wt%), K_2O (2.83–3.34 wt%), and Sr (462–729 ppm), but low Y (9.14–15.7 ppm) and Yb (0.73–1.39 ppm) with high $Mg^{\#}$ (47–55), Sr/Y (30–57) and La/Yb ratios resembling typical high–K calc-alkaline and high $Mg^{\#}$ adakitic rocks. Zircon Lu–Hf isotopes show that the studied samples have weakly juvenile zircon Lu-Hf isotopes (εHf(t) = 1.80–4.03) with older model age (1.00–1.14 Ga). The relative low content of Cr (14–59 ppm) and Ni (8–30 ppm), as well as the petrological, geochemical, and Lu-Hf isotopic data, indicates that the Mogetong adakitic rocks were generated by partial melting of thickened lower crust with a certain contribution of the underplated mantle-derived magma in slab break-off setting. This study shows that the Late Triassic adakitic magmatism in East Kunlun orogen may be the response of tectonic transition from oceanic subduction to post–subduction extension, and the reworking of ancient continental crust with subsequent variable crust-mantle magma mixing is the major mechanism of continental crust evolution in the Paleo–Tethyan orogenic belt.

Keywords: East Kunlun, magmatism, adakitic rocks, paleo-tethyan, tectonic evolution

INTRODUCTION

The East Kunlun orogen, one composite Tethyan tectonic belt in the Northern Tibet Plateau, contains large–scale Permian–Triassic granitoid batholiths and coeval volcanic rocks and thus constitutes a giant magmatic arc (Xiong et al., 2014; Zhang et al., 2021; Zhong et al., 2021). The East Kunlun magmatic arc records the subduction of the Paleo–Tethyan oceanic lithosphere and the subsequent syn–collision and post–collisional extension, which is the ideal window to understand the tectonic evolution, magma–related mineralization, and crustal growth of Paleo–Tethyan orogenic belt and to understand the crustal growth mechanism and orogeny of Tibetan Plateau (Xiong et al., 2012, 2014, 2019; Huang et al., 2014; Li et al., 2015, 2018). However, the petrogenesis and tectonic settings of these Paleo–Tethyan

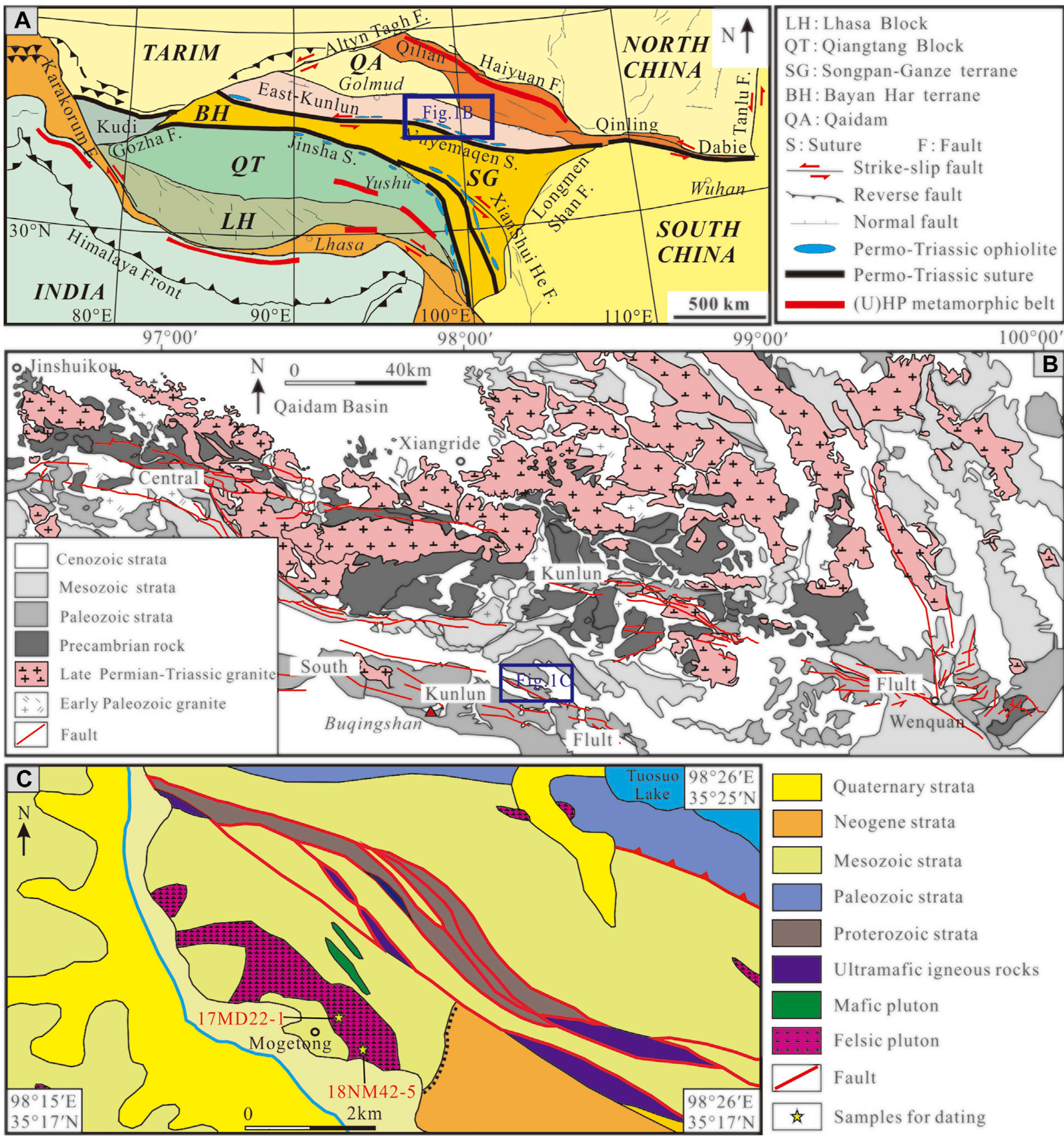

FIGURE 1 | (A) Tectonic outline of the Tibetan Plateau showing the location of East Kunlun orogen (after Roger et al., 2004); **(B)** Simplified geological map of the eastern section of East Kunlun showing the distribution of Permian-Triassic granites (after Xiong et al., 2014); **(C)** Simplified geological map of the studied Mogetong pluton.

TABLE 1 | Compilation of geochronological age data for Triassic magmatic rocks associated mineralization in East Kunlun.

Region/Mining area	Deposit type	Dating sample	Dating method	Age (Ma)	Reference
Tawenchahan	Skarn-type Fe-Cu-Zn deposit	Muscovite	$39Ar-^{40}Ar$	229.9 ± 3.5	Tian et al. (2013)
Yazigou	Skarn-type Fe-Mo deposit	Molybdenite	Re-Os isochron	210.1 ± 4.8	Feng et al. (2010)
Hutouya	Skarn-type Fe-Cu-Zn deposit	Molybdenite	Re-Os isochron	225.0 ± 4.0	Feng et al. (2011)
Suolajier	Skarn-type Cu-Mo deposit	Molybdenite	Re-Os isochron	239 ± 1.1	Feng et al. (2009)
Yazigou	Porphyry-type Cu-Mo deposit	Molybdenite	Re-Os isochron	224.7 ± 3.4	He et al. (2009)
Changshan	Porphyry-type Mo deposit	Molybdenite	Re-Os isochron	218 ± 228	Feng et al. (2010)
Yemaquan	Skarn-type Fe-Zn deposit	Phlogopite	$39Ar-^{40}Ar$	222.0 ± 1.3	Liu et al. (2017)
Shuangqing	Skarn-type Fe deposit	Molybdenite	Re-Os isochron	226.5 ± 5.1	Xia et al. (2015)
Lalingzaohuo	Skarn-type Mo-Fe deposit	Molybdenite	Re-Os isochron	214.5 ± 4.9	Wang et al. (2013)
Saishentang	Skarn-type Cu deposit	Molybdenite	Re-Os isochron	223.4 ± 1.5	Wang et al. (2015)
Naomuhun	Skarn-type Au deposit	Sericite	$39Ar-^{40}Ar$	227.8 ± 1.3	Li et al. (2017)
Shiduolong	Skarn-type Mo-Pb-Zn deposit	Molybdenite	Re-Os isochron	233.4 ± 9.6	Xia et al. (2015)

orogeny–related granitoids and volcanic equivalents are still hotly debated and several controversial models have been proposed For example, some studies propose that most Permian to Middle Triassic granitoids are formed in a subduction setting and the Kunlun Paleo–Tethyan ocean was finally closed in Late Triassic, while other studies emphasize that the Kunlun Paleo–Tethyan ocean was closed in Late Permian, and the Late Permian–Triassic granitoids all are generated in post–collisional setting, while some scholars even propose that the Paleo–Tethyan oceanic subduction lasted until the Late Triassic or Jurassic (Huang et al., 2014; Xiong et al., 2014; Chen et al., 2015, 2017; Ding et al., 2015; Li et al., 2015, 2018; Liu et al., 2017; Dong et al., 2018; Yu et al., 2020).

Recently, some studies reveal that Triassic adakites or adakitic rocks were developed in East Kunlun orogen (Yuan et al., 2009; Xiong et al., 2014; Chen et al., 2017; Zhang et al., 2017; Liang et al., 2021; Zhong et al., 2021), providing a special probe to unravel the tectonic–magmatic evolution of East Kunlun Paleo–Tethyan orogeny, since the adakites or adakitic rocks are unique with distinct geochemical signatures (e.g., high Sr/Y ratios and low Y and Yb) and can be formed in certain tectonic settings (Defant and Drummond, 1990; Martin et al., 2005; Castillo, 2012). Early studies show that adakites can be formed by partial melting of the subducted oceanic slab (Defant and Drummond, 1990; Castillo, 2012), melting of the thickened lower crust (Petford and Gallagher, 2001; Chung et al., 2003; Hou et al., 2011; Yu et al., 2018, 2019), melting of delaminated lower crust with mixing with mantle material (Xu et al., 2002; Wang et al., 2007a), magma mixing between mafic and felsic magma and differentiation of mantle–derived magma by fractional crystallization of hornblende and/or garnet (Qin et al., 2010; Foley et al., 2013). Thus, identifying the petrogenetic types of adakitic rocks and constraining their magmatic ages and tectonic settings is the key to revealing the tectonic–magmatic evolutionary history and crustal growth mechanism of Paleo–orogenic belt.

In this study, new petrological, geochronological, and geochemical data for a Late Triassic adakitic pluton in East Kunlun orogen are presented. Since previous case studies focus on the Middle Triassic adakitic rocks in East Kunlun orogen, the petrogenesis and tectonic setting of Late Triassic adakitic rocks remain unknown. Thus, the aim of this study is to: 1) comprehensively characterize the geochemical affinities of the Late Triassic adakitic rocks in East Kunlun orogen, and 2) reveal their petrogenesis and geodynamic implications for the Triassic tectonic–magmatic evolution of East Kunlun orogen. Collectively, this dataset aims to advance the understanding of the Paleo–Tethyan orogeny, magmatism–related metallization and crustal growth in Northern Tibet Plateau.

GEOLOGICAL SETTING

The East Kunlun Orogenic Belt (EKOB), located in northwestern China, extends east–west for up to 1,500 km, is bounded by the Qaidam Basin to the north, the Bayan Har–Songpan–Ganzi block to the south, the Qinling–Dabie orogenic belt to the east and the NE–trending Altyn Tagh fault to the west (**Figure 1A**; Xiong et al., 2015; Yu et al., 2018; Liu et al., 2021; Peng et al., 2021). Based on the central and south Kunlun faults, the EKOB can be divided into the North East Kunlun terrane and the South East Kunlun terrane (**Figure 1B**). The EKOB is part of the Paleo–Tethyan tectonic domain, and the Kunlun A'nyemaqen ophiolite belt represents the missing Paleo–Tethys ocean (Yang et al., 1996; Bian et al., 2004). Previous studies indicate that the Kunlun A'nyemaqen Paleo–Tethys oceanic slab began to subduct beneath the Kunlun terrane in the late Permian, but when and how did the ocean close remains a great debate. Due to the Paleo–Tethys oceanic subduction and subsequent collision, large–scale late Permian to Triassic magmatism occurred in the EKOB (**Figure 1B**; Xiong et al., 2014; Yu et al., 2017; Dong et al., 2018). Furthermore, numerous late Triassic porphyry and skarn–type mineral deposits occurred during the Paleo–Tethys orogeny (**Table 1**; Xia et al., 2017; Zhang et al., 2017; Qu et al., 2019; Zhong et al., 2021), making the EKOB one of the most important polymetallic belts in China. Thus, studying the petrogenesis of late Triassic igneous rocks is not only conducive to revealing the magmatic–tectonic evolution of EKOB, but also conducive to understanding the metallogeny background of late Triassic porphyry or skarn–type deposits.

SAMPLING AND PETROGRAPHY

The studied Mogetong pluton is located in the south Kunlun terrane and exposes it as a small stock of about 8 km southwest to

FIGURE 2 | Field and microscope graphics of the Mogetong pluton in the East Kunlun. **(A–B)** Host quartz monzonite porphyry; **(C–D)** Mafic enclave hosted in quartz monzonite porphyry; **(E–F)** Microphotographs of the quartz monzonite porphyry and enclave, respectively. Abbreviations: Amp, amphibole; Bi, biotite; Kfs, K-feldspar; Pl, plagioclase; Q, quartz.

the Tuosuo Lake (**Figures 1B,C**). The studied pluton consists of quartz monzonite porphyry and it intrudes into the early Triassic sandstone (**Figures 2A,B**). Mafic microgranular enclaves (MMEs) occur sporadically in the Mogetong pluton, and the MMEs are mainly composed of diorite and usually show sharp contact with the host quartz monzonite or quartz monzonite porphyry (**Figures 2C,D**).

The host quartz monzonite porphyry shows porphyritic texture with phenocryst minerals of plagioclase (5–7 vol%), K-feldspar (3–5 vol%), quartz (5–8 vol%), and biotite (2–3 vol. %). The matrix of the quartz monzonite porphyry comprises fine-grained plagioclase (40–45 vol. %), K-feldspar (25–30 vol%), quartz (8–10 vol%) and biotite (2 vol%) as well as minor accessory minerals of zircon, titanite, apatite, and opaque minerals (**Figure 2E**). While the MMEs are texturally and mineralogically different to their host rocks, showing fine-grained granitic texture with major minerals of euhedral plagioclase (45–50 vol%), hornblende (20–25 vol%), biotite (5

TABLE 2 | LA-ICP-MS zircon U-Pb data for the Mogetong quartz monzonite porphyry and enclave in the East Kunlun orogen, northern Tibetan Plateau.

Analysis	Contents		Ratios	Isotopic ratios						Isotopic ages (Ma)					
	Th	U	Th/U	207Pb/ ^{206}Pb	1σ	207Pb/ 2^{35}U	1σ	206Pb/ 238U	1σ	207Pb/ ^{206}Pb	1σ	207Pb/ 235U	1σ	206Pb/ ^{238}U	1σ
17MD11-2 (quartz monzonite porphyry)															
1	537	1,430	0.38	0.0503	0.0022	0.2404	0.0107	0.03448	0.00049	209	102	219	9	219	3
2	436	852	0.51	0.0507	0.0029	0.2382	0.0132	0.03440	0.00056	228	133	217	11	218	3
3	738	1,213	0.61	0.0507	0.0034	0.2391	0.0155	0.03375	0.00049	228	156	218	13	214	3
4	298	576	0.52	0.0549	0.0056	0.2497	0.0235	0.03406	0.00097	409	236	226	19	216	6
5	552	1,133	0.49	0.0528	0.0065	0.2442	0.0279	0.03374	0.00077	320	288	222	23	214	5
6	317	609	0.52	0.0482	0.0056	0.2242	0.0256	0.0335	0.0008	109	252	205	21	212	5
7	395	746	0.53	0.0497	0.0031	0.2335	0.0147	0.0337	0.0005	189	144	213	12	213	3
8	354	709	0.50	0.0609	0.0044	0.2848	0.0195	0.0345	0.0009	639	157	254	15	219	5
9	463	992	0.47	0.0504	0.0035	0.2404	0.0163	0.0342	0.0007	217	156	219	13	217	4
10	403	837	0.48	0.0512	0.0042	0.2382	0.0181	0.0344	0.0007	250	189	217	15	218	4
11	464	896	0.52	0.0517	0.0067	0.2435	0.0283	0.0341	0.0010	272	274	221	23	216	6
12	558	1,057	0.53	0.0499	0.0032	0.2300	0.0146	0.0334	0.0005	187	150	210	12	212	3
13	332	639	0.52	0.0517	0.0056	0.2433	0.0275	0.0342	0.0010	272	51	221	22	217	6
14	423	763	0.55	0.0517	0.0049	0.2387	0.0210	0.0342	0.0007	272	218	217	17	217	4
15	547	733	0.75	0.0505	0.0044	0.2353	0.0206	0.0336	0.0006	217	5	215	17	213	4
16	626	784	0.80	0.0512	0.0030	0.2336	0.0133	0.0338	0.0005	256	140	213	11	214	3
17	444	900	0.49	0.0531	0.0044	0.2404	0.0205	0.0332	0.0010	345	195	219	17	211	6
18	652	1,610	0.40	0.0527	0.0044	0.2509	0.0198	0.0345	0.0006	322	186	227	16	218	4
19	480	1,077	0.45	0.0519	0.0034	0.2402	0.0147	0.0339	0.0006	280	155	219	12	215	4
20	321	710	0.45	0.0534	0.0057	0.2439	0.0206	0.0345	0.0011	346	241	222	17	219	7
21	250	493	0.51	0.0535	0.0095	0.2445	0.0407	0.0337	0.0012	354	357	222	33	214	8
22	648	1,151	0.56	0.0498	0.0026	0.2307	0.0117	0.0336	0.0004	187	120	211	10	213	3
23	314	658	0.48	0.0529	0.0068	0.2404	0.0291	0.0336	0.0012	328	97	219	24	213	8
18NM42-4 (enclave)															
1	510	791	1.02	0.0506	0.0027	0.2316	0.0123	0.0330	0.0004	233	121	211	10	209	3
2	315	568	1.11	0.0537	0.0056	0.2472	0.0250	0.0336	0.0007	367	237	224	20	213	4
3	458	876	0.41	0.0512	0.0036	0.2384	0.0167	0.0337	0.0007	250	165	217	14	214	4
4	527	1,016	0.74	0.0510	0.0030	0.2339	0.0137	0.0332	0.0006	243	137	213	11	210	4
5	601	1,032	0.41	0.0494	0.0031	0.2297	0.0136	0.0339	0.0005	169	148	210	11	215	3
6	448	837	0.10	0.0502	0.0032	0.2356	0.0147	0.0335	0.0006	211	146	215	12	213	4
7	603	1,068	0.68	0.0498	0.0035	0.2301	0.0159	0.0329	0.0006	187	165	210	13	208	4
8	608	1,112	0.03	0.0499	0.0030	0.2300	0.0142	0.0329	0.0006	191	134	210	12	208	4
9	425	773	0.54	0.0504	0.0029	0.2264	0.0118	0.0331	0.0005	217	133	207	10	210	3
10	564	931	0.72	0.0504	0.0039	0.2330	0.0171	0.0334	0.0006	213	178	213	14	212	4
11	673	935	0.43	0.0520	0.0022	0.2380	0.0099	0.0332	0.0004	287	98	217	8	211	3
12	491	816	0.63	0.0510	0.0031	0.2448	0.0157	0.0342	0.0006	239	136	222	13	217	3
13	311	580	0.40	0.0541	0.0035	0.2557	0.0147	0.0352	0.0006	372	151	231	12	223	4
14	498	922	1.24	0.0548	0.0039	0.2555	0.0170	0.0341	0.0006	467	159	231	14	216	4
15	622	1,241	1.03	0.0553	0.0040	0.2463	0.0160	0.0329	0.0007	433	168	224	13	209	4

vol%) as well as subhedral K-feldspar (10–15 vol%) and anhedral quartz (5 vol%) (**Figure 2F**). Nine representative samples were sampled for the geochemical study, and two samples, i.e., the quartz monzonite porphyry (sample 17MD22–1) and the MMEs (sample 18NM42–4) were collected for zircon U–Pb dating at N35°18.8′, E98°18.9’.

ANALYTICAL METHODS

The studied samples were collected from fresh outcrops and zircons were separated by heavy liquid and magnetic methods. Zircon grains were photographed with an optical microscope and the internal structures were analyzed by cathodoluminescence (CL). Zircon U–Pb dating was finished by laser ablation–inductively coupled plasma–mass spectrometry (LA–ICP–MS) at the Stake Key Laboratory of Geological Processes and Mineral Resources (GPMR), China University of Geosciences, Wuhan. Laser sampling was performed using a GeoLas 2005 system with a spot size of 32 μm. An Agilent 7500a ICP–MS instrument was used to acquire ion signal intensities. Helium was applied as a carrier gas, and Ar was used as the make–up gas and mixed with the carrier gas via a T–connector before entering the ICP source. Nitrogen was added to the central gas flow (Ar + He) of the Ar plasma to lower the detection limits and improve precision. Concordia diagrams and weighted–mean ages were made by Isoplot/Ex_ver3 (Ludwig, 2003). Data were processed using *ICPMSDataCal* (Liu et al., 2010). The detailed operating conditions for the laser system and ICP–MS instrument are as described by Liu et al. (2013).

Whole–rock samples were crushed in a corundum jaw crusher (to 60 mesh). About 60 g of this material was powdered in an

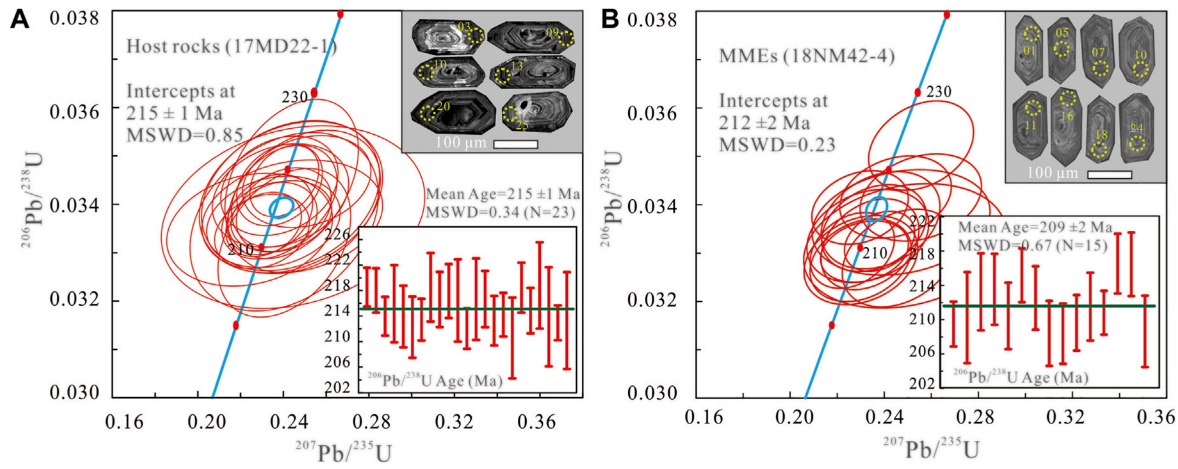

FIGURE 3 | Zircon U-Pb concordia diagrams and reprehensive zircon CL images for the Mogetong quartz monzonite porphyry and MMEs.

agate ring mill to<200 mesh for whole–rock geochemical analysis. The major element analysis was conducted by standard X–ray fluorescence (XRF) methods, using a Shimadzu Sequential 1800 spectrometer at the GPMR. Precision is <4% and accuracy is <3% for the major element. The detailed techniques for the major element analysis were described by Ma et al. (2012). Trace elements were analyzed using an Agilent 7500a ICP–MS at GPMR. The samples were digested by HF + HNO_3 acid in Teflon bombs. Analyses of USGS standards (AGV–2, BHVO–2, BCR–2, and RGM2) indicate an accuracy of <5–10% for most trace elements. The sample digestion procedures and ICP–MS methods are as described by Liu et al. (2008).

In situ zircon Hf isotopic analysis was performed on the dated zircon domains using an excimer (193 nm wavelength) laser ablation inductively coupled plasma mass spectrometer (LA–MC–ICP–MS) at the State Key Laboratory of Continental Dynamics, Northwest University, Xi'an, China. The GeoLas 200 M laser–ablation system (MicroLas, Göttingen, Germany) was used for the laser ablation experiments. Helium was used as carrier gas transporting the ablated sample from the ablation cell to the ICP–MS torch. A 44 μm beam size was adopted in this study with a laser pulse frequency of 10 Hz. Zircon standards 91,500, GJ–1 and Monastery were used as references. The detailed analytical technique for this method was described by Yuan et al. (2008).

RESULTS

Zircon U–Pb Geochronology

All the studied zircons are euhedral, elongate, inclusion–free, and transparent. LA–ICP–MS zircon U–Pb data are given in **Table 2**, and representative zircon CL images and analyzed spots are shown in **Figure 3**. The zircons have euhedral crystal shapes and exhibit oscillatory or broad zoning. The zircons from the quartz monzonite porphyry (sample 17MD22–1) and MMEs (18NM42–4) all have high concentrations of Th and U and high Th/U ratios (0.38–0.80 and 0.49–0.85, respectively; **Table 2**), indicating their magmatic origin (Corfu et al., 2003).

Twenty-three analyses from sample 17MD22–1 yield concordant 206Pb/^{238}U ages of 211–219 Ma (**Table 2**) and a weighted mean age of 215 ± 1 Ma (MSWD = 0.34; **Figure 3A)**, which is identical to their Tera-Wasserburg U–Pb lower intercept age of 215 ± 1 Ma (MSWD = 0.85), were within the acceptable error. Thus, the 215 ± 1 Ma is interpreted as the crystallization age of the Mogetong quartz monzonite porphyry. Fifteen analyses from sample 18NM42–4 exhibit 206Pb/^{238}U show ages ranging from 208 Ma to 223 Ma and yield a concordant age of 212 ± 2 Ma with a weighted mean age of 209 ± 2 Ma (MSWD = 0.67; **Figure 3B** and **Table 2**). These two ages were consistent with the acceptable error, so the concordant age of 212 ± 2 Ma represented the crystallization age of MMEs. Thus, the above results indicate the zircons of MMEs have nearly identical crystallization age to that of the zircons in host rocks.

Whole–Rock Geochemistry

Geochemical analyses of representative samples are listed in **Table 3**. The Mongetong quartz monzonite porphyries have a narrow range of SiO_2 contents (63.31–65.74 wt%), moderate contents of TiO_2 (0.47–0.68 wt%), Al_2O_3 (15.19–16.02 wt%), FeO^T (2.54–3.83 wt%), MgO (1.33–2.67 wt%), and high contents of total alkaline (Na_2O + K_2O = 7.03–8.19 wt%). The quartz monzonite porphyries define a sub–alkaline trend in the total alkalis–silica (TAS) diagram (**Figure 4A**) and a high-K calc–alkaline trend with high K_2O contents (2.83–3.34 wt%; **Table 3** and **Figure 4B**). These samples are metaluminous with A/CNK values of 0.94–1.02 (**Table 3**), and it is worth noting that the Mongetong quartz monzonite porphyries exhibit high $Mg^{\#}$ values (47–55). The MMEs show mafic-intermediate composition with SiO_2 of 49.73–56.94 wt%, TiO_2 of 1.14–1.20 wt%, FeO^T of 6.00–7.93 wt%, MgO of 3.88–3.91 wt %, and exhibit much higher Na_2O/K_2O values (2.18–3.23) and similar $Mg^{\#}$ (47–54).

TABLE 3 | Whole-rock major and trace element compositions of the studied pluton in the EKOB, northern Tibetan Plateau.

Samples	17MD18-4	17MD19-1	17MD20-1	18NM42-5	18NM42-6	18NM42-7	18NM42-8	18NM42-4	18NM42-9
Rock types	quartz monzonite porphyry							enclave	
Major element (wt%)									
SiO_2	64.32	65.74	63.55	63.35	63.43	63.69	63.31	56.94	49.73
TiO_2	0.53	0.47	0.64	0.67	0.68	0.65	0.64	1.20	1.14
Al_2O_3	15.19	15.74	15.40	15.88	16.02	15.66	15.52	16.17	19.59
FeO^T	3.02	2.54	3.83	3.54	3.63	3.31	3.32	6.00	7.93
MnO	0.05	0.04	0.07	0.05	0.05	0.06	0.05	0.12	0.16
MgO	1.98	1.33	2.67	1.78	1.79	2.15	2.25	3.88	3.91
CaO	2.45	2.57	2.26	2.52	2.60	3.41	3.19	3.67	10.29
Na_2O	5.11	5.00	4.52	4.48	4.51	3.89	4.12	4.66	2.23
K_2O	3.08	2.83	3.30	3.28	3.34	3.14	3.19	2.14	0.69
P_2O_5	0.21	0.20	0.25	0.30	0.31	0.25	0.24	0.46	0.25
LOI	3.65	3.10	2.84	2.97	2.95	2.86	3.43	3.07	2.27
Total	98.85	98.88	98.85	98.68	98.78	98.96	98.76	98.98	99.05
K_2O/Na_2O	0.60	0.57	0.73	0.73	0.74	0.81	0.77	0.46	0.31
$Mg^\#$	54	48	55	47	47	54	55	54	47
Trace element (ppm)									
Li	36.9	26.1	60.8	42.4	43.6	64.6	72.0	55.5	34.0
Be	2.35	2.08	2.06	2.51	2.70	2.38	2.19	2.25	1.10
Sc	6.92	4.22	8.48	6.03	6.17	7.75	7.67	14.6	20.8
V	46.1	27.3	60.6	32.9	34.0	52.2	49.9	116	200
Cr	47.7	13.6	59.1	14.1	17.0	37.9	37.7	60	14.5
Co	10.0	6.42	12.7	9.38	9.64	11.3	11.0	22.1	19.7
Ni	25.4	8.22	30.1	10.3	10.6	22.5	21.9	38.0	8.06
Cu	6.94	5.74	10.73	5.00	4.83	10.7	9.4	96.5	8.3
Zn	44.4	56.3	51.1	63.5	62.4	52.2	50.9	77.6	97.0
Ga	17.8	18.4	18.2	18.8	18.4	18.7	18.0	19.6	19.4
Rb	104	92.4	118	135	131	100	113	89.7	29.1
Sr	557	524	599	515	462	729	660	770	668
Y	12.9	9.14	15.2	15.4	15.7	14.1	13.8	24.1	21.7
Zr	166	174	173	196	193	172	163	194	105
Nb	19.7	17.9	25.6	26.1	26.4	18.8	18.5	29.7	5.47
Mo	0.33	0.22	0.92	0.18	0.18	0.38	0.25	0.42	0.13
Sn	1.82	1.50	2.49	1.94	2.27	1.65	1.80	2.48	0.92
Cs	4.45	7.07	5.59	5.66	5.21	5.46	7.12	5.46	11.2
Ba	811	881	1,019	800	812	877	752	582	213
La	39.1	35.6	47.0	49.0	39.2	34.0	33.2	44.6	13.1
Ce	70.4	62.4	86.3	91.0	73.3	62.9	61.5	84.5	31.0
Pr	7.64	6.66	8.96	9.35	7.84	6.71	6.46	9.25	4.20
Nd	26.0	22.7	30.9	32.5	28.7	24.5	24.3	35.0	19.0
Sm	4.33	3.63	5.19	5.10	4.94	4.41	4.36	6.36	4.38
Eu	1.06	1.02	1.32	1.29	1.32	1.17	1.14	1.71	1.40
Gd	3.34	2.79	3.99	3.77	3.62	3.37	3.26	5.33	4.34
Tb	0.46	0.35	0.54	0.51	0.50	0.46	0.45	0.77	0.65
Dy	2.37	1.74	2.90	2.78	2.86	2.60	2.58	4.54	3.92
Ho	0.42	0.31	0.56	0.51	0.53	0.50	0.48	0.82	0.76
Er	1.19	0.80	1.52	1.40	1.40	1.36	1.31	2.35	2.17
Tm	0.18	0.12	0.21	0.21	0.20	0.19	0.18	0.32	0.31
Yb	1.13	0.73	1.39	1.24	1.37	1.25	1.18	2.04	1.99
Lu	0.17	0.12	0.22	0.20	0.19	0.18	0.18	0.32	0.31
Hf	4.05	4.06	4.30	4.58	4.49	4.12	3.93	4.51	2.67
Ta	1.43	1.23	1.71	1.80	1.77	1.23	1.16	1.79	0.27
Tl	0.48	0.47	0.66	0.66	0.53	0.48	0.48	0.38	0.17
Pb	21.5	20.6	20.1	22.8	19.4	18.5	16.7	17.0	17.2
Th	12.5	9.82	14.6	14.0	12.1	9.23	8.99	9.76	1.50
∑REE	171	148	206	214	182	158	154	222	109
(La/Yb)N	23.3	32.9	22.9	26.7	19.3	18.4	19.0	14.7	4.5
δEu	0.85	0.98	0.89	0.90	0.95	0.93	0.93	0.90	0.98

*Note: Total Fe as FeO^T; $Mg^\#$ = 100*molar MgO/(MgO + FeO); δEu = $Eu_N/(Sm_N*Gd_N)^{1/2}$.*

The Mongetong quartz monzonite porphyries are characterized by enrichment in light rare earth elements (LREEs) and depletion in heavy rare earth elements (HREEs) [$(La/Yb)_N$ = 14.73–32.87; **Figure 5A**]. The host rocks and MMEs all display high total REEs (RREE = 148–222 ppm) and slightly negative Eu anomalies (Eu/Eu* = 0.8–0.9). To sum up, the host rocks and MMEs exhibit

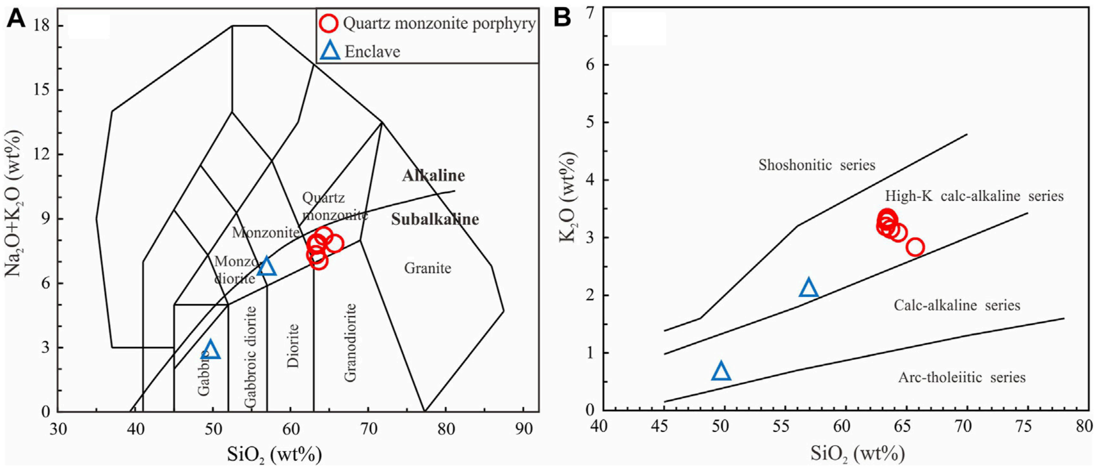

FIGURE 4 | (A) TAS classification and nomenclature diagram (Middlemost, 1994); **(B)** SiO_2 versus K_2O diagram for the studied rocks (Peccerillo and Taylor, 1976).

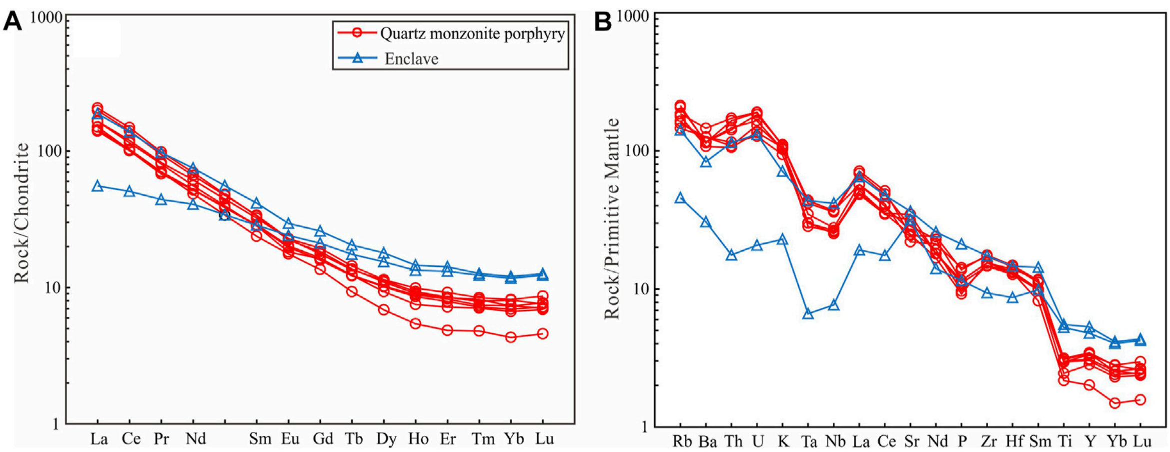

FIGURE 5 | (A) Chondrite-normalized REE patterns [normalization values after Taylor and Mclennan (1985)] and **(B)** Primitive mantle-normalized trace element spider diagrams [normalization values after Sun and McDonough (1989)] for the studied Mogetong pluton.

TABLE 4 | Zircon Lu-Hf isotopic compositions for the Mogetong quartz monzonite porphyry in EKOB, northern Tibetan Plateau.

Spots	176Yb/ ^{177}Hf	2σ	176Lu/ ^{177}Hf	2σ	176Hf/ 177Hf	2σ	(^{176}Hf/ ^{177}Hf)$_i$	$\varepsilon_{Hf(t)}$	2σ	T_{DM1}(Ga)	T_{DM2} (Ga)
17MD22-1 (quartz monzonite porphyry, t = 215 Ma)											
1	0.037963	0.000498	0.001003	0.000018	0.282744	0.000027	0.282740	3.57	0.94	0.72	1.03
2	0.039701	0.000682	0.000992	0.000024	0.282694	0.000028	0.282690	1.80	0.97	0.79	1.14
3	0.037362	0.000340	0.001033	0.000015	0.282738	0.000024	0.282734	3.37	0.84	0.73	1.04
4	0.030288	0.000296	0.000760	0.000007	0.282731	0.000031	0.282728	3.16	1.09	0.73	1.05
5	0.031988	0.000344	0.000808	0.000011	0.282725	0.000029	0.282722	2.95	1.00	0.74	1.07
6	0.025587	0.000049	0.000641	0.000002	0.282703	0.000033	0.282700	2.19	1.14	0.77	1.12
7	0.033537	0.000051	0.000839	0.000003	0.282716	0.000027	0.282712	2.61	0.96	0.76	1.09
8	0.046984	0.000145	0.001152	0.000005	0.282734	0.000029	0.282729	3.20	1.00	0.74	1.05
9	0.026424	0.000038	0.000649	0.000001	0.282733	0.000030	0.282730	3.23	1.05	0.73	1.05
10	0.026513	0.000050	0.000646	0.000002	0.282695	0.000030	0.282693	1.92	1.05	0.78	1.13
11	0.039158	0.000119	0.000987	0.000005	0.282740	0.000028	0.282736	3.43	0.99	0.73	1.04
12	0.032284	0.000085	0.000802	0.000003	0.282698	0.000029	0.282695	1.99	1.02	0.78	1.13
13	0.028618	0.000043	0.000704	0.000002	0.282724	0.000029	0.282722	2.94	1.03	0.74	1.07
14	0.042915	0.000034	0.001048	0.000001	0.282715	0.000029	0.282711	2.57	1.01	0.76	1.09
15	0.048916	0.000041	0.001180	0.000002	0.282757	0.000024	0.282753	4.03	0.83	0.71	1.00

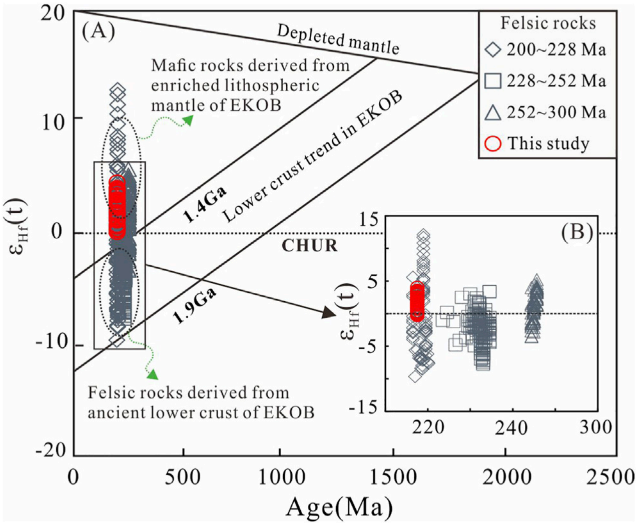

FIGURE 6 | Zircon εHf(t) versus age diagram. Data sources for the Triassic felsic igneous rocks in East Kunlun are as follows: Xiong et al. (2012, 2014, 2019), Huang et al. (2014), Li et al. (2015, 2018).

similar trace elements patterns, exhibiting overall enrichment in large ion lithophile elements (LILE; e.g., Th, U, K) and LREE, and depleted in high field strength elements (HFSE; e.g., Nb, Ta, Ti and *p*; **Figure 5B**). Importantly, the quartz monzonite porphyries have high contents of Sr (462–729 ppm) and Ba (752–1,019 ppm), but low contents of Y (9.14–15.7 ppm) and Yb (0.73–1.39 ppm) and low values of Sr/Y (30–57) and La/Yb (27–49), resembling typical adakites or adakitic rocks.

Zircon Lu–Hf Isotope

Zircon Lu–Hf isotopic data are shown in **Table 4**. Fifteen spots were analyzed for the sample 17MD22–1 and all the analyses have similar initial 176Hf/^{177}Hf values of between 0.282690 and 0.282753. The zircons exhibit weakly juvenile Hf isotopes (εHf(t) = 1.80–4.03), with Hf isotopic model ages ranging from 1.00 Ga to 1.14 Ga (**Table 4**; **Figure 6**).

DISCUSSION

Magma Source and Petrogenesis

Several Triassic adakitic rocks have been reported in the East Kunlun orogenic belt, and most of them exhibit crystallization age of Middle–Late Triassic (Yuan et al., 2009; Xiong et al., 2014; Chen et al., 2017; Zhang et al., 2017; Liang et al., 2021; Zhong et al., 2021), thus providing a window to constrain the magma-tectonic evolution of East Kunlun Paleo-Tethyan orogen. The studied Mongetong quartz monzonite porphyries have adakitic affinities, e.g., intermediate SiO_2, high Sr, low Y and Yb contents, and high Sr/Y and La/Yb ratios (**Table 3**; **Figure 7**). Their high SiO_2 contents and moderate ($CaO + Na_2O$) values show that the studied pluton is a high–silicon adakite like the other Triassic adakitic rocks in East Kunlun (**Table 3**; Martin et al., 2005; Castillo, 2012).

Adakites or adakitic rocks were originally recognized in Cenozoic Aleutian island arcs where their generation is associated with the subduction of relatively young (≤25 Ma) oceanic slabs (Defant and Drummond, 1990). Slab melting of subducted oceanic slabs has been proposed to account for the genesis of adakitic rocks (Defant and Drummond, 1990; Drummond et al., 1996; Ma et al., 2014; Zheng et al., 2021). However, several other mechanisms have also been proposed to account for the origin of adakitic rocks, such as partial melting of the thickened basaltic lower crust (Atherton and Petford, 1993; Chung et al., 2003; Wang et al., 2007a; Yu et al., 2018, Yu et al., 2019), partial melting of mantle peridotite metasomatized by slab melt under water–bearing condition (Martin et al., 2005; Castillo, 2008), magma mixing between felsic and basaltic magmas (Qin et al., 2010; Foley et al., 2013), low–pressure fractional

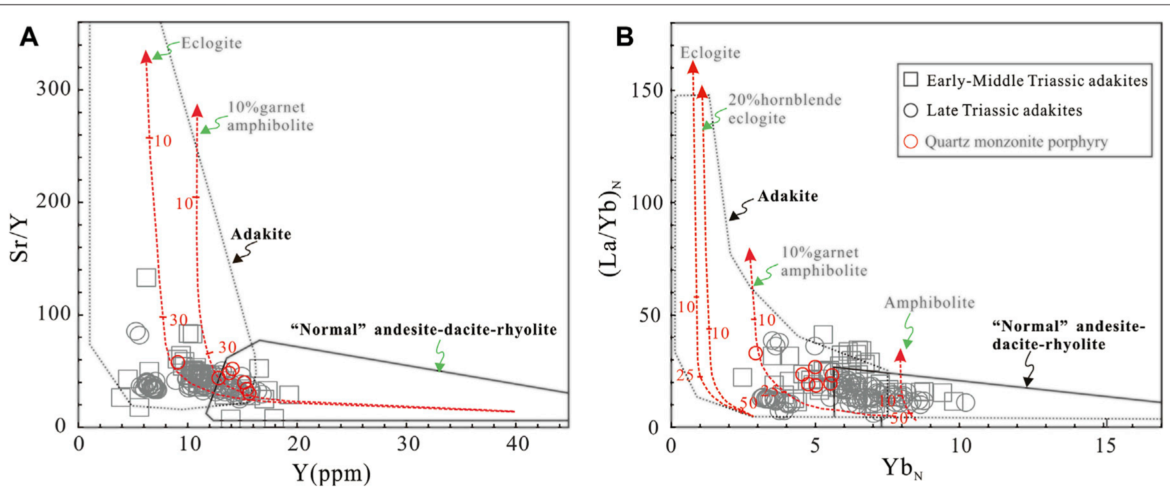

FIGURE 7 | (A) Sr/Y versus Y and **(B)** $(La/Yb)_N$ versus $(Yb)_N$ diagrams for the studied adakitic rocks (Defant and Drummond, 1990; Martin et al., 2005). Data sources for the adakites are from Yuan et al. (2009), Ding et al. (2014), Xia et al. (2014), Xiong et al. (2014), Chen et al. (2017), Shao et al. (2017), Zhang et al. (2017), Yin et al. (2020), Li et al. (2021), Liang et al. (2021), Zhong et al. (2021) and this study.

crystallization of parental basaltic magmas (Castillo, 2012; Chen et al., 2016), and high–pressure fractional crystallization (involving garnet) of mafic magmas (Martin et al., 2005; Macpherson et al., 2006; Chiaradia, 2009). Adakitic magmas derived from melting of subducted oceanic slabs usually have the following geochemical characteristics: depleted or relative juvenile radiogenic isotopes with young model ages, and sodic series with relatively low K_2O content and K_2O/Na_2O values (Defant and Drummond, 1990; Martin et al., 2005; Wang et al., 2007b). The Mogetong adakitic quartz monzonite porphyries have old zircon Hf isotopic model ages (1.00–1.14 Ga; **Figure 6**) and they exhibit high K_2O/Na_2O values (0.57–0.81) with high-K calc-alkaline affinities (**Figure 4**, **8A**), which is identical to the felsic rocks derived from partial melting of the ancient lower continental crust in East Kunlun (Xiong et al., 2014; Ding et al., 2015; Li et al., 2021). Moreover, the studied adakitic rocks have weak juvenile zircon Hf isotopes (εHf(t) = 1.80–4.03), which is much lower than the East Kunlun Paleo-Tethyan MORB (εHf(t) = 15–20; Huang et al., 2014; Hu et al., 2016), and it is unlikely that the Mogetong adakitic quartz monzonite porphyries were derived from basaltic slab melting. Besides, phase equilibrium modeling and experimental studies reveal that melting of either pristine or altered oceanic basaltic slab usually leads to the generation of high-SiO_2 and strongly sodic adakitic melts (Hernández-Uribe et al., 2019; Li et al., 2022), and the melts are usually rich in SiO_2 (>68 wt%) and Al_2O_3 (>18 wt%), but poor in FeO and MgO (<0.2 wt%), which is not the case of the studied Mogetong adakitic rocks (e.g., potassium, low contents of Al_2O_3 (15.19–16.02 wt%) and moderate contents of SiO_2 (63.31–65.74 wt%) and MgO (1.33–2.67 wt%); **Figures 4**, **8** and **Table 3**). Besides, the partial melts from fresh or hydrothermally altered MORB usually have $(La/Yb)_N$ >194 and $(La/Yb)_N$ >15, respectively, and those from altered MORB are characterized by strong negative Th anomalies (Hernández-Uribe et al., 2019), which are not the case of the studied Mogetong adakitic rocks (e.g., $(La/Yb)_N$ = 18–33; enrichment in Th; **Figure 5B** and **Table 3**).

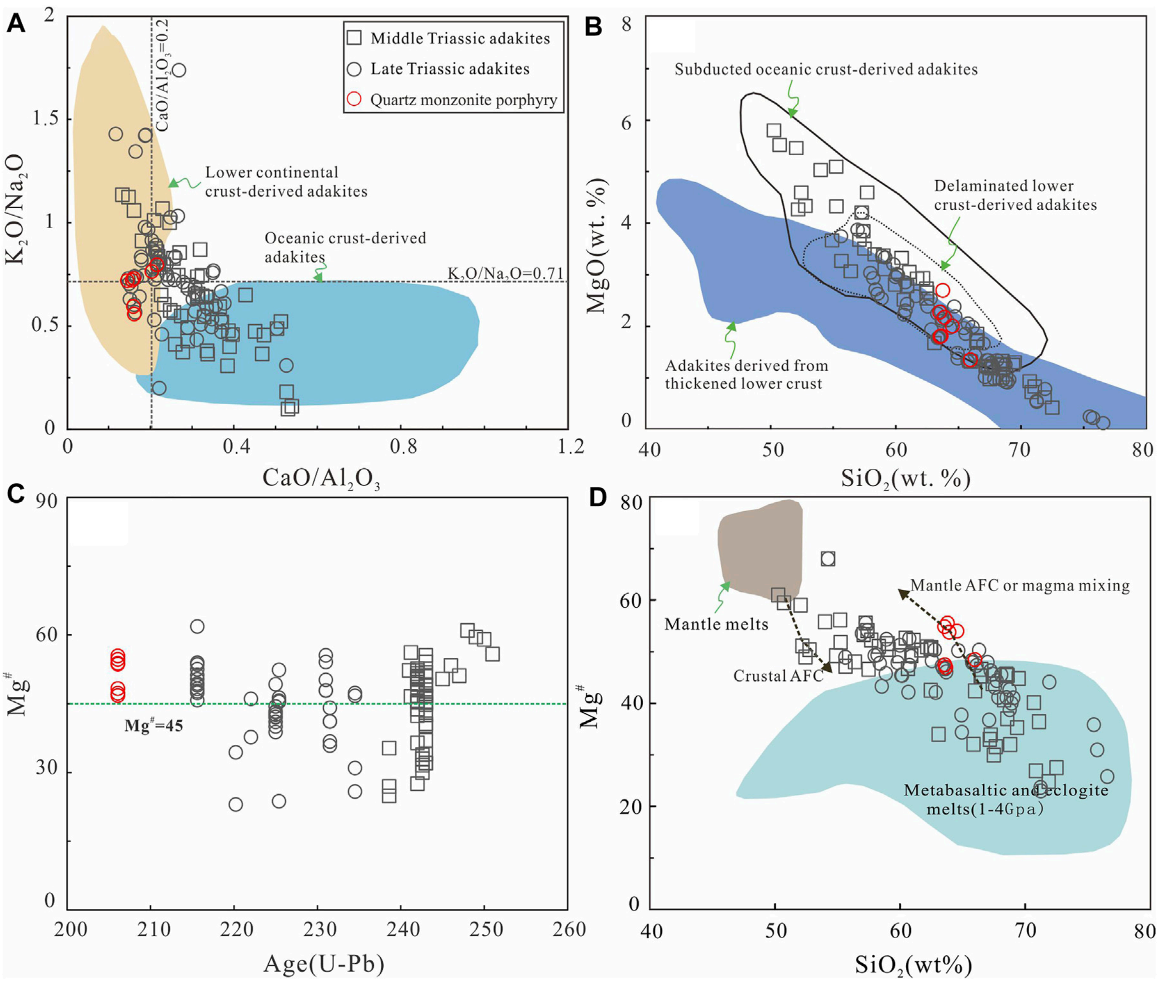

FIGURE 8 | Geochemical characteristics of major elements for the studied adakitic rocks and published data for other Triassic adakites in EKOB. Mantle melts, mantle AFC curves, and crust AFC curves are from Stern and Kilian (1996). Data for metabasaltic and eclogite experimental melts (1–4.0 GPa) are from Rapp et al. (1999) and references therein. K_2O/Na_2O versus CaO/Al_2O_3 and MgO versus SiO_2 diagrams are from Wang et al. (2006), Chen et al. (2018) and references therein. Data sources are same to **Figure 7**.

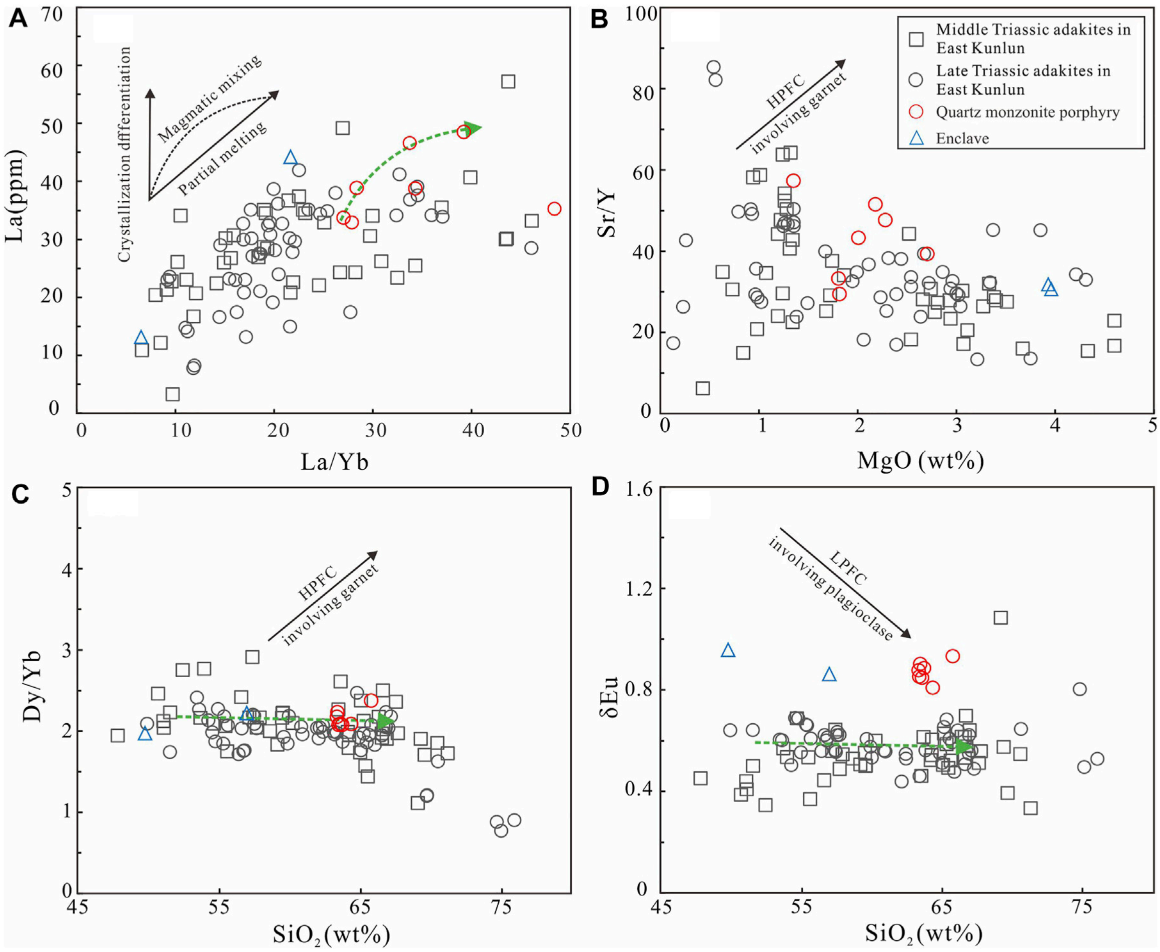

FIGURE 9 | (A) La versus La/Yb, **(B)** Sr/Y versus MgO, **(C)** Dy/Yb versus SiO_2, and **(D)** δEu versus SiO_2 (Drummond et al., 1996) diagrams showing the compositional evolution of the studied Mogetong adakitic quartz monzonite porphyries and enclaves. Abbreviations: HPFC = high-pressure fractional crystallization; LPFC = low-pressure fractional crystallization. Data sources are same to **Figure 7**.

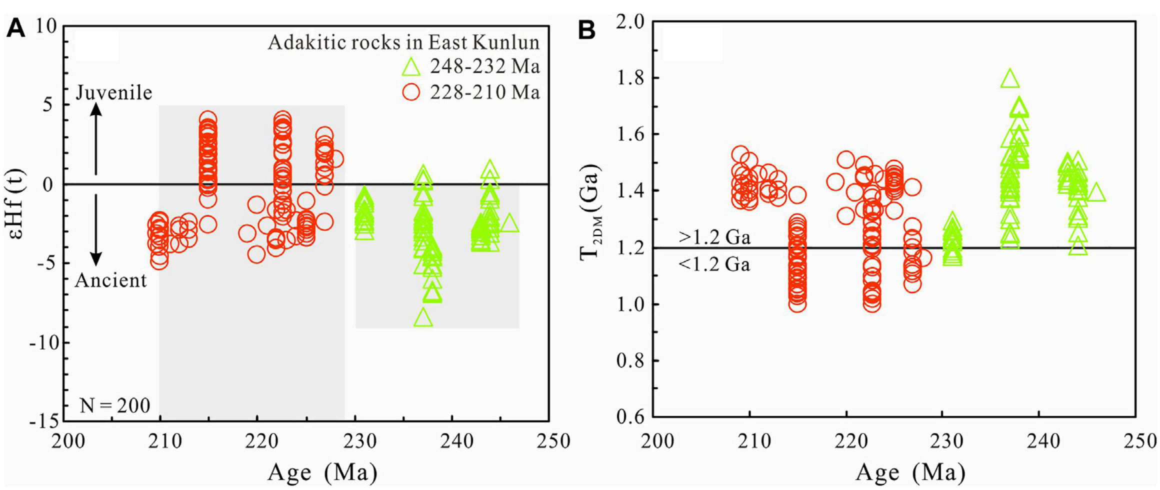

FIGURE 10 | Temporal evolution of zircon εHf(t) and Hf isotope model age for the Triassic adakites in East Kunlun orogenic belt. Data sources are same to **Figure 7**.

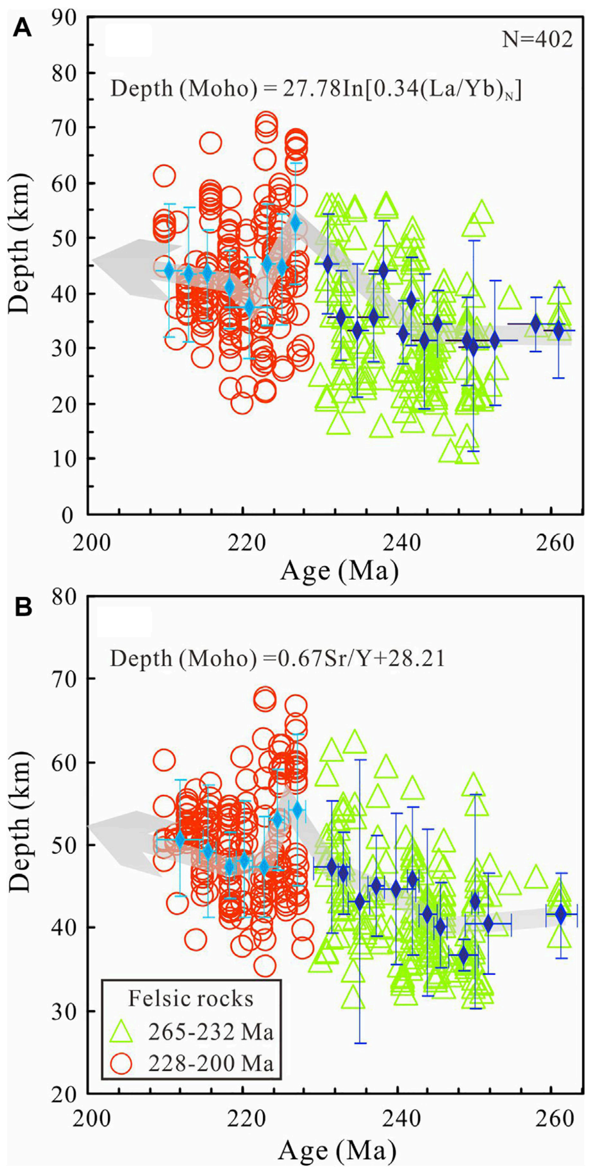

FIGURE 11 | Temporal changes of calculated crustal thickness from $(La/Yb)_N$ **(A)** and Sr/Y **(B)** for the East Kunlun during the Triassic. Crustal thickness with uncertainty is calculated by using the correlation equations in Chapman et al. (2015). Data sources are from Xiong et al. (2012), Huang et al. (2014), Xiong et al. (2014), Chen et al. (2015), Ding et al. (2015), Li et al. (2015), Xiong et al. (2016), Chen et al. (2017), Liu et al. (2017), Dong et al. (2018), Li et al. (2018), Xiong et al. (2019), Yu et al. (2020).

Besides, adakitic magmas derived from partial melting of thickened basaltic lower crust without crust-mantle interaction would have relatively low MgO contents and $Mg^{\#}$ values, and these melts are usually characterized by low $Mg^{\#}$ values (<40) regardless of the melting degree (Atherton and Petford, 1993; Castillo, 2012). The Mogetong adakitic quartz monzonite porphyries have high $Mg^{\#}$ values ($Mg^{\#}$ = 47–55; **Figures 8B–D**), which is distinct from the thickened basaltic lower crust–derived adakitic rocks. Conversely, adakitic rocks formed by high-pressure partial melting of continental crust would have relatively high $(Gd/Yb)_N$ ratios (>5.8) (Huang and He, 2010), however, this is not the case of the Mogetong adakitic rocks ($(Gd/Yb)_N$ = 2.14–3.09). The Mogetong adakitic quartz monzonite porphyries show partial melting trends rather than fractional crystallization trends (**Figure 9A**), indicating fractional crystallization of parental basaltic magmas may not be the most critical factor accounting for the genesis of the studied rocks. Typical adakitic rocks derived by fractional crystallization of basaltic magmas usually have low SiO_2 content (Martin et al., 2005; Chiaradia, 2009; Castillo, 2012), which is different from the Mogetong adakitic rocks as well as other Triassic adakitic rocks in East Kunlun (**Figures 8B,D**). In addition, given that high–pressure fractional crystallization involving garnet usually causes a decrease in HREEs and Y contents, the Sr/Y and Dy/Yb ratios in the residual magmas should increase with increasing SiO_2 and MgO content (Macpherson et al., 2006; Laurent et al., 2013). However, the Mogetong adakitic quartz monzonite porphyries do not show such a trend in the Sr/Y versus MgO and Dy/Yb versus SiO_2 diagrams (**Figures 9B,C**). During low–pressure fractional crystallization involving hornblende and plagioclase, the net effect of hornblende and plagioclase fractionation is a decrease in δEu with increasing SiO_2 content, which is observed in most typical arc adakites (Martin et al., 2005; Moyen, 2009), but is not present in the Mogetong adakitic rocks (**Figure 9D**).

Here, we propose that magma mixing between felsic and basaltic magmas is the most possible mechanism accounting for the generation of the studied Mogetong quartz monzonite porphyries. Their moderate SiO_2 contents (63.31–65.74 wt%) but high $Mg^{\#}$ values (47–55), as well as weak juvenile Hf isotopes, support the model of crust-mantle interaction (**Figures 6**, **8D**). The studied rocks exhibit much more depleted zircon Hf isotope than those derived from the ancient continent crust (**Figure 6**), indicating the significant contribution of mantle-derived magma. Furthermore, the high field strength element ratios of these samples also support the crust–mantle mixing model, such as their Nb/Ta values (average 14.87) ranging between the average continental crust (Nb/Ta = 11; Sun and McDonough, 1989) and the average primary mantle (Nb/Ta = 17.7; Taylor and McLennan, 1985). The correlation trend between La and La/Yb also confirms the major role of magma mixing (**Figure 9A**). Besides, the presence of the MMEs further indicate the occurring of magma mixing, although several petrogenetic models have been proposed for the origin of MMEs (Qin et al., 2010; Xiong et al., 2012, 2014), including 1) restites, 2) cognate fragments of cumulates, 3) quenched mafic melts derived from the mantle, and 4) mixing of mafic and felsic magmas. The MMEs in the Late Triassic Mogetong pluton have granitic textures with euhedral plagioclase, biotite and amphibole, subhedral K-feldspar, and anhedral quartz (**Figure 2F**), which does not support the cumulates and quenched mafic melts model but indicates that the MMEs crystallized from a melt. The MMEs have mafic-intermediate compositions with slightly silica contents of 49.73–56.94 wt%, which also contradicts the idea of the MMEs being cognate fragments of mafic cumulates and quenched mafic melts. Moreover, the euhedral magmatic

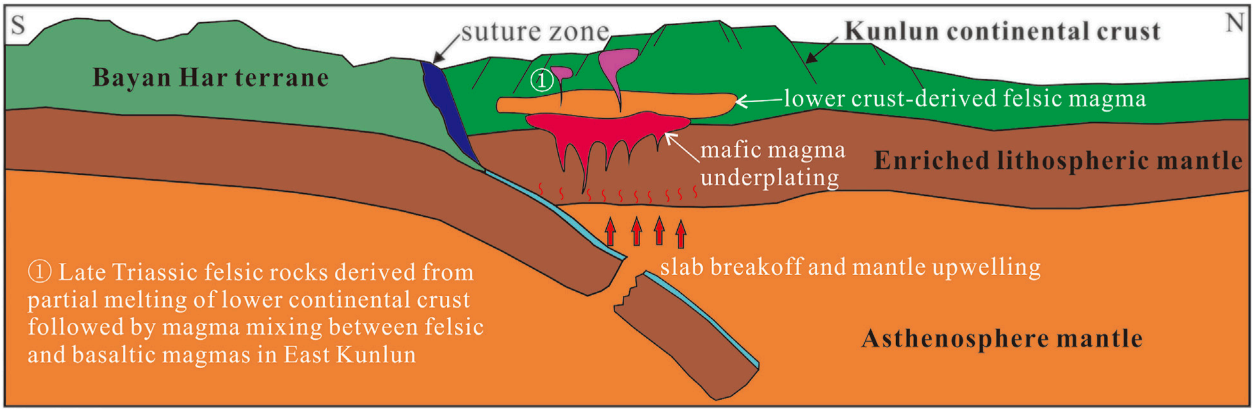

FIGURE 12 | Schematic cartoon showing the possible Paleo-Tethyan tectono-magma dynamic model for the generation of the studied Late Triassic adakitic pluton in the East Kunlun.

zircons with clear igneous oscillatory and identical U-Pb ages to their host rocks also preclude the restite model, but support the magma mixing model (**Figure 3**). These features, as well as the fact of different trace elemental patterns between the MMEs and their host rocks, support the magma mixing model for the origin of the studied Mogetong pluton and MMEs, and the contemporary most mafic enclave (sample 18NM42–9) could represent the basaltic end-member. The Mogetong adakitic rocks have variable and positive values of εHf(t) (1.80–4.03) with moderate $Mg^{\#}$ (47–54), which also indicate a mantle component in their source. However, petrological and geochemical evidence indicates that the contribution of mantle material is not significant. For example, the MMEs are sporadically developed in the Mogetong adakitic pluton and the host rocks have low contents of Cr (14–59 ppm) and Ni (8–30 ppm). More importantly, the Hf isotopes of the studied rocks are much lower than those of the underplating primitive basaltic magma (εHf(t) = 8–15; Hu et al., 2018) or the Paleo-Tethyan MORB in the East Kunlun (εHf(t) = 15–20; Huang et al., 2014; Hu et al., 2016). The continental crust-like Nb/Ta values of the Mogetong adakitic rocks (14–16) are much lower than the MORB-like Nb/Ta values of the MMEs (17–20), which also support this suggestion (Taylor and McLennan, 1985; Sun and McDonough, 1989).

Implications for Tectonic Setting and Continent Crustal Evolution

The tectonic evolution of East Kunlun Paleo-Tethyan orogen during the late Paleozoic to early Mesozoic is still controversial and the key problem is the timing of the tectonic transition from oceanic slab subduction to continental collision (Li et al., 2013a, Li et al., 2018; Liu et al., 2017; Dong et al., 2018; Xiong et al., 2019; Yu et al., 2020; Zhang et al., 2021). Since there is an obvious genetic link between the magma source and tectonic setting of adakitic rocks, the detailed petrogenesis study could contribute to our understanding of the evolution of Triassic East Kunlun Paleo–Tethyan orogen. The above discussion on the petrogenesis shows that the Mogetong adakitic magma was originated from crust-mantle mixing, indicating that there was a significant contribution of mantle material in the Late Triassic. This is further supported by the zircon Hf isotopes of Triassic adakites (**Figure 10**). A comprehensive comparison of the Hf isotopic composition of Triassic adakites in East Kunlun orogen shows that there is a significant juvenile trend in the Late Triassic (**Figure 10**). Besides, the published data shows that there were two episodic adakitic magmatisms in the East Kunlun orogen, i.e. the Middle Triassic and Late Triassic, however, the latter is the main metallogeny stage for the porphyry–and/or skarn–type deposits (Yuan et al., 2009; Xiong et al., 2014; Chen et al., 2017; Zhang et al., 2017; Liang et al., 2021; Zhong et al., 2021). The above characteristics all indicate that the East Kunlun was in a special tectonic setting during the Late Triassic.

Through an integrated geochemical comparison among the Triassic adakites in East Kunlun orogen, we propose a revised tectonic evolution model for the East Kunlun Paleo-Tethyan orogen. As mentioned above, the crust-mantle magma mixing is the main genetic mechanism for the Late Triassic adakites in the East Kunlun, thus, revealing the properties of the late Triassic mantle-derived magma is the key to understanding the tectonic setting of Late Triassic adakitic magmatism. Previous studies have shown that mid-ocean ridge subduction, slab break–off, and slab roll–back and lithospheric delamination could trigger the underplating of mantle-derived magma and subsequent crustal melting and magma mixing (Martin et al., 2005; Wang et al., 2007b; Tang et al., 2010; Keller and Schoene, 2018). At present, however, Triassic mafic magmatic rocks with N–MORB affinities, back-arc basalts, back-arc basin, and the temporal–spatial migration trend of Triassic magmatism have not been found or reported in the East Kunlun orogen, precluding the model of mid-ocean ridge subduction and slab rollback (Hu et al., 2016; Xiong et al., 2019). Besides, lithospheric delamination-related magma will interact with mantle peridotite, forming adakitic magmas with high contents of Ni and Cr (Huang et al., 2008; Qin et al., 2010), but the Mogetong adakitic quartz monzonite porphyries do not exhibit high Cr and Ni contents.

Meanwhile, recent studies have shown that whole-rock Sr/Y and La/Yb ratios of felsic rocks can effectively reveal continent crustal thickness (Chapman et al., 2015). To eliminate mafic rocks generated in the mantle and to avoid the influence of magma mixing and/or highly fractional crystallization on the calculation results, the data set was filtered to include rocks with moderate SiO_2 content (55–68 wt%) and MgO content (one to four wt%). Data with Rb/Sr > 0.2 or Rb/Sr < 0.05 were further discarded, providing a trace elemental filter for mantle-derived rocks or rocks formed by melting of pre-existing metasedimentary framework rocks (Chapman et al., 2015). Using these empirical correlations, we investigate temporal variations of crustal thickness in the East Kunlun orogen, and our results suggest that crustal thickness increased during the Early-Middle Triassic and remained constant during the Late Triassic (**Figure 11**). The calculated results also indicate that the continent crustal thinning of East Kunlun did not occur during the Late Triassic, precluding the model of lithospheric delamination in the Late Triassic. Here, we propose that slab break-off may occur in the Late Triassic, which induced the underplating of mantle-derive mafic magma and promoted the melting of thickened crust and subsequent magma mixing (**Figure 12**). The Late Triassic OIB-like mafic igneous rocks and mafic dyke swarms in East Kunlun may be the response of slab break-off (Hu et al., 2016; Xiong et al., 2019). The slab break–off model also matches the linear distribution of Late Triassic adakites along the Eastern Kunlun Paleo-Tethyan suture zone (Dong et al., 2018). Besides, mantle-derived mafic magma underplating in the break–off model not only provides heat, but also provides ore-forming metals, which may be the key to the Late Triassic mineralization flare-up in the Eastern Kunlun orogen (Zhang et al., 2017; Zhong et al., 2021). Several pieces of evidence support the idea that late Triassic Mogetong adakites were formed in a post–subduction extensional setting, such as mantle–derived high Nb–Ta rhyolite (213 Ma; Ding et al., 2011), crustal–derived shoshonitic volcanic rocks (228–215 Ma; Hu et al., 2016), and coeval mafic dyke (226–210 Ma; Xiong et al., 2011, 2019; Hu et al., 2016; Liu et al., 2017). The angular unconformity between Late Triassic land facies volcanic-sedimentary rocks, e.g., Babaoshan Formation red clastic sedimentary rocks and E'lashan Formation volcanic rocks, and underlying sea-land facies strata is the records of tectonic transition from oceanic subduction to post-subduction collision or extension (Li et al., 2013a).

This study also suggests that the reworking of the ancient lithosphere and subsequent magma mixing are the important mechanisms for the generation of granitoids and continental crust growth. It is previously well accepted that the growth and evolution of the continental crust in orogen is mostly dominated by felsic magmatism, such as the Central Asian Orogenic Belt (Li et al., 2013b; Kröner et al., 2014), and the late Paleozoic to early Mesozoic felsic igneous rocks in the Central Asian Orogenic Belt are characterized by much depleted Sr–Nd–Hf isotopic compositions, indicating juvenile materials played a key role in crustal growth in Central Asia (Jahn et al., 2000; Li et al., 2013b; Xiao and Santosh, 2014). However, our study shows that the isotopic compositions of the Triassic adakites in East Kunlun are different from those of the Central Asian Orogenic Belt but identical to those derived from the melting of Precambrian continental crust with a contribution of mantle-derived magma, implying a different crustal evolution mechanism in East Kunlun (Xiong et al., 2012, 2014; Yu et al., 2017; Li et al., 2018). We propose that the reworking of a dominantly ancient continental crust with certain addition of lithospheric mantle materials is another major mechanism for the generation of felsic igneous rocks and the evolution of the continental crust.

CONCLUSION

(1) LA–ICP–MS zircon U–Pb geochronology studies show that the Mogetong quartz monzonite porphyries and enclaves in East Kunlun have identical crystallization ages of ca. 215–212 Ma. The Mogetong quartz monzonite porphyries are characterized by high SiO_2, K_2O and Sr, but low Y and Yb with high $Mg^{\#}$ values, Sr/Y and La/Yb ratios, resembling typical high–K calc–alkaline and high $Mg^{\#}$ adakitic rocks.
(2) Petrology, geochemistry and zircon Lu–Hf isotope reveals that the Mogetong adakitic quartz monzonite porphyries were generated by partial melting of thickened lower crust with a certain contribution of magma mixing in slab break-off setting.
(3) This study shows that the Late Triassic adakitic magmatism in East Kunlun orogen may be the response of tectonic transition from oceanic subduction to post–subduction extension and the reworking of ancient continental crust with subsequent crust-mantle magma mixing is the major mechanism of continental crust evolution in Paleo–Tethyan orogenic belt.

DATA AVAILABILITY STATEMENT

The original contributions presented in the study are included in the article/Supplementary Material, further inquiries can be directed to the corresponding authors.

AUTHOR CONTRIBUTIONS

JG, QX, and FX contributed to conception and design of the study and wrote the first draft of the manuscript. WW and DY helped writing the manuscript, provided comments and suggestions, and revised the manuscript.

FUNDING

This study was financially supported by National Natural Science Foundation of China (No. 41602049) and Research Project of Chengdu University of Technology (No. 2021ZF11412).

ACKNOWLEDGMENTS

We thank Wen Zhang and Keqing Zong for their contribution to the laboratory work.

REFERENCES

Atherton, M. P., and Petford, N. (1993). Generation of Sodium-Rich Magmas from Newly Underplated Basaltic Crust. *Nature* 362, 144–146. doi:10.1038/362144a0

Bian, Q.-T., Li, D.-H., Pospelov, I., Yin, L.-M., Li, H.-S., Zhao, D.-S., et al. (2004). Age, Geochemistry and Tectonic Setting of Buqingshan Ophiolites, North Qinghai-Tibet Plateau, China. *J. Asian Earth Sci.* 23 (4), 577–596. doi:10.1016/j.jseaes.2003.09.003

Castillo, P. R. (2012). Adakite Petrogenesis. *Lithos* 134-135, 304–316. doi:10.1016/j.lithos.2011.09.013

Castillo, P. R. (2008). Origin of the Adakite-High-Nb basalt Association and its Implications for Postsubduction Magmatism in Baja California, Mexico. *Geol. Soc. America Bull.* 120 (3-4), 451–462. doi:10.1130/B26166.1

Chapman, J. B., Ducea, M. N., DeCelles, P. G., and Profeta, L. (2015). Tracking Changes in Crustal Thickness during Orogenic Evolution with Sr/Y: An Example from the North American Cordillera. *Geology* 43 (10), 919–922. doi:10.1130/G36996.1

Chen, J., Wei, J., Fu, L., Li, H., Zhou, H., Zhao, X., et al. (2017). Multiple Sources of the Early Mesozoic Gouli Batholith, Eastern Kunlun Orogenic Belt, Northern Tibetan Plateau: Linking Continental Crustal Growth with Oceanic Subduction. *Lithos* 292-293, 161–178. doi:10.1016/j.lithos.2017.09.006

Chen, S., Niu, Y., Li, J., Sun, W., Zhang, Y., Hu, Y., et al. (2016). Syn-Collisional Adakitic Granodiorites Formed by Fractional Crystallization: Insights from Their Enclosed Mafic Magmatic Enclaves (Mmes) in the Qumushan Pluton, North Qilian Orogen at the Northern Margin of the Tibetan Plateau. *Lithos* 248-251, 455–468. doi:10.1016/j.lithos.2016.01.033

Chen, S., Niu, Y., and Xue, Q. (2018). Syn-Collisional Felsic Magmatism and Continental Crust Growth: A Case Study from the North Qilian Orogenic Belt at the Northern Margin of the Tibetan Plateau. *Lithos* 308-309, 53–64. doi:10.1016/j.lithos.2018.03.001

Chen, X., Gehrels, G., Yin, A., Zhou, Q., and Huang, P. (2015). Geochemical and Nd-Sr-Pb-O Isotopic Constrains on Permo-Triassic Magmatism in Eastern Qaidam Basin, Northern Qinghai-Tibetan Plateau: Implications for the Evolution of the Paleo-Tethys. *J. Asian Earth Sci.* 114 (4), 674–692. doi:10.1016/j.jseaes.2014.11.013

Chiaradia, M. (2009). Adakite-Like Magmas from Fractional Crystallization and Melting-Assimilation of Mafic Lower Crust (Eocene Macuchi Arc, Western Cordillera, Ecuador). *Chem. Geology.* 265 (3-4), 468–487. doi:10.1016/j.chemgeo.2009.05.014

Chung, S.-L., Liu, D., Ji, J., Chu, M.-F., Lee, H.-Y., Wen, D.-J., et al. (2003). Adakites from Continental Collision Zones: Melting of Thickened Lower Crust beneath Southern Tibet. *Geol* 31 (11), 1021–1024. doi:10.1130/g19796.1

Corfu, F., Hanchar, J. M., Hoskin, P. W. O., and Kinny, P. (2003). 16. Atlas of Zircon Textures. *Rev. Mineralogy Geochem.* 53, 469–502. doi:10.1515/9781501509322-019

Defant, M. J., and Drummond, M. S. (1990). Derivation of Some Modern Arc Magmas by Melting of Young Subducted Lithosphere. *Nature* 347 (6294), 662–665. doi:10.1038/347662a0

Ding, Q.-F., Jiang, S.-Y., and Sun, F.-Y. (2014). Zircon U-Pb Geochronology, Geochemical and Sr-Nd-Hf Isotopic Compositions of the Triassic Granite and Diorite Dikes from the Wulonggou Mining Area in the Eastern Kunlun Orogen, NW China: Petrogenesis and Tectonic Implications. *Lithos* 205, 266–283. doi:10.1016/j.lithos.2014.07.015

Ding, Q., Liu, F., and Yan, W. (2015). Zircon U–Pb Geochronology and Hf Isotopic Constraints on the Petrogenesis of Early Triassic Granites in the Wulonggou Area of the Eastern Kunlun Orogen, Northwest China. *Int. Geol. Rev.* 57, 1–20. doi:10.1080/00206814.2015.1029541

Ding, S., Huang, H., Niu, Y. L., Zhao, Z. D., Yu, X. H., and Mo, X. X. (2011). Geochemistry, Geochronology and Petrogenesis of East Kunlun High Nb-Ta Rhyolites. *Acta Petrol. Sin.* 27, 3603–3614.

Dong, Y., He, D., Sun, S., Liu, X., Zhou, X., Zhang, F., et al. (2018). Subduction and Accretionary Tectonics of the East Kunlun Orogen, Western Segment of the Central China Orogenic System. *Earth-Science Rev.* 186, 231–261. doi:10.1016/j.earscirev.2017.12.006

Drummond, M. S., Defant, M. J., and Kepezhinskas, P. K. (1996). Petrogenesis of Slab-Derived Trondhjemite-Tonalite-Dacite/adakite Magmas. *Earth Environ. Sci. Trans. R. Soc. Edinb.* 87, 205–215. doi:10.1130/0-8137-2315-9.20510.1017/s0263593300006611

Feng, C. Y., Li, D. S., Wu, Z. S., Li, J. H., Zhang, Z. Y., Zhang, A. K., et al. (2010). Major Types, Time-Apace Distribution and Metallogeneses of Polymetallic Deposits in the Qimantage Metallogenic belt , Eastern Kunlun Area. *Northwest. Geology.* 43 (4), 10–17. (in Chinese with English abstract).

Feng, C. Y., Wang, X. P., Shu, X. F., Zhang, A. K., Xiao, Y., Liu, J. N., et al. (2011). Isotopic Chronology for Hutouya Skarn-type lead–zinc Polymetallic Metallogenic District in the Qimantage Area, Qinghai Province, and its Geological Significance. *J. Jilin Univ. (Earth Sci. Ed.* 41 (6), 1806–1817. (in Chinese with English abstract).

Feng, C. Y., Li, D. S., Qu, W. J., Du, A. D., Wang, S., Su, S. S., et al. (2009). Re-Os Isotopic Dating of Molybdenite from the Suolajier Skarn-type Copper-Molybdenum Deposit of Qimantage Mountain in Qinghai Province and its Geological Significance. *Rock Mineral. Anal.* 8 (3), 223–227. (in Chinese with English abstract).

Foley, F. V., Pearson, N. J., Rushmer, T., Turner, S., and Adam, J. (2013). Magmatic Evolution and Magma Mixing of Quaternary Adakites at Solander and Little Solander Islands, New Zealand. *J. Petrol.* 54 (4), 703–744. doi:10.1093/petrology/egs082

He, S. Y., Li, D. S., Li, L. L., Qi, L. Y., and He, S. F. (2009). Re-Os Age of Molybdenite from the Yazigou Copper (Molybdenum) Mineralized Area in Eastern Kunlun of Qinghai Province, and its Geological Significance. *Geotecton. Metallog.* 33 (2), 236–242. (in Chinese with English abstract).

Hernández-Uribe, D., Hernández-Montenegro, J. D., Cone, K. A., and Palin, R. M. (2019). Oceanic Slab-Top Melting during Subduction: Implications for Trace-Element Recycling and Adakite Petrogenesis. *Geology* 48, 216–220. doi:10.1130/G46835.1

Hou, Z., Zhang, H., Pan, X., and Yang, Z. (2011). Porphyry Cu (–Mo–Au) Deposits Related to Melting of Thickened Mafic Lower Crust: Examples from the Eastern Tethyan Metallogenic Domain. *Ore Geol. Rev.* 39 (1), 21–45. doi:10.1016/j.oregeorev.2010.09.002

Hu, C. B., Li, M., Zha, X. F., Gao, X. F., and Li, T. (2018). Genesis and Geological Significance of Late Paleozoic Mantle-Derived Magmatism in Qimantag, East Kunlun: A Case Study of Intrusion in Yingzhuagou. *Earth Sci.* 43 (12), 4334–4349. (in Chinese with English abstract). doi:10.3799/dqkx.2018.120

Hu, Y., Niu, Y., Li, J., Ye, L., Kong, J., Chen, S., et al. (2016). Petrogenesis and Tectonic Significance of the Late Triassic Mafic Dikes and Felsic Volcanic Rocks in the East Kunlun Orogenic Belt, Northern Tibet Plateau. *Lithos* 245, 205–222. doi:10.1016/j.lithos.2015.05.004

Huang, F., and He, Y. (2010). Partial Melting of the Dry Mafic Continental Crust: Implications for Petrogenesis of C-type Adakites. *Chin. Sci. Bull.* 55 (22), 2428–2439. doi:10.1007/s11434-010-3224-2

Huang, F., Li, S., Dong, F., He, Y., and Chen, F. (2008). High-Mg Adakitic Rocks in the Dabie Orogen, Central China: Implications for Foundering Mechanism of Lower Continental Crust. *Chem. Geol.* 255 (1), 1–13. doi:10.1016/j.chemgeo.2008.02.014

Huang, H., Niu, Y., Nowell, G., Zhao, Z., Yu, X., Zhu, D.-C., et al. (2014). Geochemical Constraints on the Petrogenesis of Granitoids in the East Kunlun Orogenic Belt, Northern Tibetan Plateau: Implications for Continental Crust Growth through Syn-Collisional Felsic Magmatism. *Chem. Geology.* 370, 1–18. doi:10.1016/j.chemgeo.2014.01.010

Jahn, B.-m., Wu, F., and Chen, B. (2000). Granitoids of the Central Asian Orogenic Belt and Continental Growth in the Phanerozoic. *Trans. R. Soc. Edinb. Earth Sci.* 91 (1-2), 181–193. doi:10.1130/0-8137-2350-7.181

Keller, B., and Schoene, B. (2018). Plate Tectonics and Continental Basaltic Geochemistry throughout Earth History. *Earth Planet. Sci. Lett.* 481, 290–304. doi:10.1016/j.epsl.2017.10.031

Kröner, A., Kovach, V., Belousova, E., Hegner, E., Armstrong, R., Dolgopolova, A., et al. (2014). Reassessment of Continental Growth during the Accretionary History of the Central Asian Orogenic Belt. *Gondwana Res.* 25 (1), 103–125. doi:10.1016/j.gr.2012.12.023

Laurent, O., Doucelance, R., Martin, H., and Moyen, J.-F. (2013). Differentiation of the Late-Archaean Sanukitoid Series and Some Implications for Crustal Growth: Insights from Geochemical Modelling on the Bulai Pluton, Central Limpopo Belt, South Africa. *Precambrian Res.* 227, 186–203. doi:10.1016/j.precamres.2012.07.004

Li, H., Hermann, J., and Zhang, L. (2022). Melting of Subducted Slab Dictates Trace Element Recycling in Global arcs. *Sci. Adv.* 8 (25), h2166. (in Chinese with English abstract). doi:10.1126/sciadv.abh2166

Li, J. C., Kon, H. L., Li, Y. Z., Namkha, N., Jia, Q. Z., and Guo, X. Z. (2017). Ar-Ar Age of Altered Sericite, Zircon U-Pb Age of Quartz Diorite and Geochemistry of the Naomuhun Gold deposit, East Kunlun. *Acta Geologica Sinica* 91, 979–991.

Li, R. B., Pei, X. Z., Li, Z. C., Sun, Y., Pei, L., Chen, G. C., et al. (2013a). Regional Tectonic Transformation in East Kunlun Orogenic Belt in Early Paleozoic: Constraints from the Geochronology and Geochemistry of Helegangnaren Alkali-Feldspar Granite. *Acta Geologica Sinica-English Edition* 87 (2), 333–345.

Li, R., Pei, X., Pei, L., Li, Z., Chen, G., Chen, Y., et al. (2018). The Early Triassic Andean-type Halagatu Granitoids Pluton in the East Kunlun Orogen, Northern Tibet Plateau: Response to the Northward Subduction of the Paleo-Tethys Ocean. *Gondwana Res.* 62, 212–226. doi:10.1016/j.gr.2018.03.005

Li, S., Wang, T., Wilde, S. A., and Tong, Y. (2013b). Evolution, Source and Tectonic Significance of Early Mesozoic Granitoid Magmatism in the Central Asian Orogenic Belt (Central Segment). *Earth-Science Rev.* 126, 206–234. doi:10.1016/j.earscirev.2013.06.001

Li, X., Huang, X., Luo, M., Dong, G., and Mo, X. (2015). Petrogenesis and Geodynamic Implications of the Mid-triassic Lavas from East Kunlun, Northern Tibetan Plateau. *J. Asian Earth Sci.* 105, 32–47. doi:10.1016/j.jseaes.2015.03.009

Li, Z.-C., Pei, X.-Z., Bons, P. D., Li, R.-B., Pei, L., Chen, G.-C., et al. (2021). Petrogenesis and Tectonic Setting of the Early-Middle Triassic Subduction-Related Granite in the Eastern Segment of East Kunlun: Evidences from Petrology, Geochemistry, and Zircon U-Pb-Hf Isotopes. *Int. Geology. Rev.* 64 (5), 698–721. doi:10.1080/00206814.2021.1875268

Liang, Y., Xia, R., Ma, Y., Zhao, E., and Guo, W. (2021). Petrogenesis and Tectonic Significance of Late Triassic Baishiya Granodiorite Porphyries in the Dulan Area, Eastern Segment of the East Kunlun Orogenic Belt, China. *Geol. J.* 56 (1), 284–297. doi:10.1002/gj.3961

Liu, B., Ma, C.-Q., Huang, J., Wang, L.-X., Zhao, S.-Q., Yan, R., et al. (2017). Petrogenesis and Tectonic Implications of Upper Triassic Appinite Dykes in the East Kunlun Orogenic Belt, Northern Tibetan Plateau. *Lithos* 284-285, 766–778. doi:10.1016/j.lithos.2017.05.016

Liu, D., Li, H., Ge, C., Bai, M., Wang, Y., Pan, J., et al. (2021). Northward Growth of the West Kunlun Mountains: Insight from the Age-Elevation Relationship of New Apatite Fission Track Data. *Front. Earth Sci.* 9. doi:10.3389/feart.2021.784812

Liu, J. N., Feng, C. Y., Zhao, Y. M., Li, D. X., Xiao, Y., Zhou, J. H., et al. (2013). Characteristics of Intrusive Rock, Metasomatites, Mineralization, and Alteration in Yemaquan Skarn Fe–Zn Polymetallic deposit, Qinghai Province. *Mineral. Deposit* 32 (1), 77–93. (in Chinese with English abstract).

Liu, Y., Gao, S., Hu, Z., Gao, C., Zong, K., and Wang, D. (2010). Continental and Oceanic Crust Recycling-Induced Melt–Peridotite Interactions in the Trans-North China Orogen: U–Pb Dating, Hf Isotopes and Trace Elements in Zircons from Mantle Xenoliths. *J. Petrol.* 51 (1-2), 537–571. doi:10.1093/petrology/egp082

Liu, Y., Hu, Z., Gao, S., Günther, D., Xu, J., Gao, C., et al. (2008). *In Situ* Analysis of Major and Trace Elements of Anhydrous Minerals by La-Icp-Ms without Applying an Internal Standard. *Chem. Geology.* 257 (1-2), 34–43. doi:10.1016/j.chemgeo.2008.08.004

Ludwig, K. R. (2003). *User's Manual for Isoplot/Ex Version 3.00: A Geochronological Toolkit for Microsoft Excel (No. 4ed.)*. Berkeley: Berkeley Geochronology Center, Special Publication.

Ma, L., Wang, B.-D., Jiang, Z.-Q., Wang, Q., Li, Z.-X., Wyman, D. A., et al. (2014). Petrogenesis of the Early Eocene Adakitic Rocks in the Napuri Area, Southern Lhasa: Partial Melting of Thickened Lower Crust during Slab Break-Off and Implications for Crustal Thickening in Southern Tibet. *Lithos* 196-197, 321–338. doi:10.1016/j.lithos.2014.02.011

Ma, Q., Zheng, J., Griffin, W. L., Zhang, M., Tang, H., Su, Y., et al. (2012). Triassic "Adakitic" Rocks in an Extensional Setting (North China): Melts from the Cratonic Lower Crust. *Lithos* 149, 159–173. doi:10.1016/j.lithos.2012.04.017

Macpherson, C. G., Dreher, S. T., and Thirlwall, M. F. (2006). Adakites without Slab Melting: High Pressure Differentiation of Island Arc Magma, Mindanao, the Philippines. *Earth Planet. Sci. Lett.* 243 (3-4), 581–593. doi:10.1016/j.epsl.2005.12.034

Martin, H., Smithies, R. H., Rapp, R., Moyen, J. F., and Champion, D. (2005). An Overview of Adakite, Tonalite-Trondhjemite-Granodiorite (Ttg), and Sanukitoid: Relationships and Some Implications for Crustal Evolution. *Lithos* 79 (1-2), 1–24. doi:10.1016/j.lithos.2004.04.048

Middlemost, E. A. K. (1994). Naming Materials in the Magma/Igneous Rock System. *Earth-sci. Rev.* 37 (3), 215–224. doi:10.1016/0012-8252(94)90029-9

Moyen, J. (2009). High Sr/Y and La/Yb Ratios: The Meaning of the "Adakitic Signature". *Lithos* 112 (3), 556–574. doi:10.1016/j.lithos.2009.04.001

Peccerillo, A., and Taylor, S. R. (1976). Geochemistry of Eocene Calc-Alkaline Volcanic Rocks from the Kastamonu Area, Northern Turkey. *Contr. Mineral. Petrol.* 58 (1), 63–81. doi:10.1007/bf00384745

Peng, Y., Yu, S., Zhang, J., Li, Y., Li, S., and Lv, P. (2021). Building a continental Arc Section: Constraints from Paleozoic Granulite-Facies Metamorphism, Anatexis, and Magmatism in the Northern Margin of the Qilian Block, Northern Tibet Plateau. *Geol. Soc. Am. Bull.* doi:10.1130/B36100.1

Petford, N., and Gallagher, K. (2001). Partial Melting of Mafic (Amphibolitic) Lower Crust by Periodic Influx of Basaltic Magma. *Earth Planet. Sc. Lett.* 193 (3-4), 483–499. doi:10.1016/s0012-821x(01)00481-2

Qin, J.-F., Lai, S.-C., Diwu, C.-R., Ju, Y.-J., and Li, Y.-F. (2010a). Magma Mixing Origin for the post-collisional Adakitic Monzogranite of the Triassic Yangba Pluton, Northwestern Margin of the South China Block: Geochemistry, Sr-Nd Isotopic, Zircon U-Pb Dating and Hf Isotopic Evidences.

Qin, J. F., Lai, S. C., Grapes, R., Diwu, C., Ju, Y. J., and Li, Y. F. (2010b). Origin of Late Triassic High-Mg Adakitic Granitoid Rocks from the Dongjiangkou Area, Qinling Orogen, Central China: Implications for Subduction of continental Crust. *Lithos* 120 (3-4), 347–367. doi:10.1016/j.lithos.2010.08.022

Qu, H., Friehauf, K., Santosh, M., Pei, R., Li, D., Liu, J., et al. (2019). Middle-Late Triassic Magmatism in the Hutouya Fe-Cu-Pb-Zn deposit, East Kunlun Orogenic Belt, NW China: Implications for Geodynamic Setting and Polymetallic Mineralization. *Ore Geology. Rev.* 113, 103088. doi:10.1016/j.oregeorev.2019.103088

Rapp, R. P., Shimizu, N., Norman, M. D., and Applegate, G. S. (1999). Reaction between Slab-Derived Melts and Peridotite in the Mantle Wedge: Experimental Constraints at 3.8 Gpa. *Chem. Geology.* 160 (4), 335–356. doi:10.1016/s0009-2541(99)00106-0

Roger, F., Malavieille, J., Leloup, P. H., Calassou, S., and Xu, Z. (2004). Timing of Granite Emplacement and Cooling in the Songpan-Garzê Fold Belt (Eastern Tibetan Plateau) with Tectonic Implications. *J. Asian Earth Sci.* 22 (5), 465–481. doi:10.1016/s1367-9120(03)00089-0

Shao, F., Niu, Y., Liu, Y., Chen, S., Kong, J., and Duan, M. (2017). Petrogenesis of Triassic Granitoids in the East Kunlun Orogenic Belt, Northern Tibetan Plateau and Their Tectonic Implications. *Lithos* 282-283, 33–44. doi:10.1016/j.lithos.2017.03.002

Stern, C. R., and Kilian, R. (1996). Role of the Subducted Slab, Mantle Wedge and Continental Crust in the Generation of Adakites from the Andean Austral Volcanic Zone. *Contrib. Mineralogy Pet.* 123 (3), 263–281. doi:10.1007/s004100050155

Sun, S.-s., and McDonough, W. F. (1989). Chemical and Isotopic Systematics of Oceanic Basalts: Implications for Mantle Composition and Processes. *Geol. Soc. Lond. Spec. Publications* 42, 313–345. doi:10.1144/gsl.sp.1989.042.01.19

Tang, G., Wang, Q., Wyman, D. A., Li, Z. X., Zhao, Z. H., Jia, X. H., et al. (2010). Ridge Subduction and Crustal Growth in the Central Asian Orogenic Belt: Evidence from Late Carboniferous Adakites and High-Mg Diorites in the Western Junggar Region, Northern Xinjiang (West China). *Chem. Geol.* 277 (3-4), 281–300. doi:10.1016/j.chemgeo.2010.08.012

Taylor, S. R., and McLennan, S. M. (1985). *The Continental Crust: Its Composition and Evolution*. Oxford: Blackwell Scientific Publications.

Tian, C. S., Feng, C. Y., Li, J. H., and Cao, D. Z. (2013). 40Ar–39Ar Geochronology of Tawenchahan Fe-Polymetallic deposit in Qimantag Mountain of Qinghai Province and its Geological Implications. *Mineral. Deposits* 3 (1), 169–176. (in Chinese with English abstract).

Wang, F. C., Chen, J., Xie, Z. Y., Li, S. P., Tan, S. X., Wang, Y. B., et al. (2013). Geological Features and Re-os Isotopic Dating of the Lalingzaohuo Molybdenum Polymetallic deposit in East Kunlun. *Geol. China.* 40 (4), 1209–1217. (in Chinese with English abstract).

Wang, H., Feng, C. Y., Li, D. X., Li, C., Ding, T. Z., and Zhou, J. H. (2015). Molybdenite Re-os Geochronology and Sulfur Isotope Geochemistry of the

Saishitang Copper Deposit,Qinghai Province. *Acta Geologica Sinica* 89 (3), 487–497. (in Chinese with English abstract).

Wang, Q., Wyman, D. A., Xu, J. F., Zhao, Z. H., Jian, P., and Zi, F. (2007a). Partial Melting of Thickened or Delaminated Lower Crust in the Middle of Eastern China: Implications for Cu-Au Mineralization. *J. Geology.* 115 (2), 149–161. doi:10.1086/510643

Wang, Q., Wyman, D. A., Xu, J., Jian, P., Zhao, Z., Li, C., et al. (2007b). Early Cretaceous Adakitic Granites in the Northern Dabie Complex, Central China: Implications for Partial Melting and Delamination of Thickened Lower Crust. *Geochimica et Cosmochimica Acta* 71 (10), 2609–2636. doi:10.1016/j.gca.2007.03.008

Wang, Q., Xu, J.-F., Jian, P., Bao, Z.-W., Zhao, Z.-H., Li, C.-F., et al. (2006). Petrogenesis of Adakitic Porphyries in an Extensional Tectonic Setting, Dexing, South China: Implications for the Genesis of Porphyry Copper Mineralization. *J. Petrol.* 47, 119–144. doi:10.1093/petrology/egi070

Xia, R., Deng, J., Qing, M., Li, W., Guo, X., and Zeng, G. (2017). Petrogenesis of Ca. 240 Ma Intermediate and Felsic Intrusions in the Nan'getan: Implications for Crust-Mantle Interaction and Geodynamic Process of the East Kunlun Orogen. *Ore Geology. Rev.* 90, 1099–1117. doi:10.1016/j.oregeorev.2017.04.002

Xia, R., Wang, C., Qing, M., Deng, J., Carranza, E. J. M., Li, W., et al. (2015). Molybdenite Re-os, Zircon U-Pb Dating and Hf Isotopic Analysis of the Shuangqing Fe-Pb-Zn-Cu Skarn deposit, East Kunlun Mountains, Qinghai Province, China. *Ore Geology. Rev.* 66, 114–131. doi:10.1016/j.oregeorev.2014.10.024

Xia, R., Wang, C., Deng, J., Carranza, E. J. M., Li, W., and Qing, M. (2014). Crustal Thickening Prior to 220Ma in the East Kunlun Orogenic Belt: Insights from the Late Triassic Granitoids in the Xiao-Nuomuhong Pluton. *J. Asian Earth Sci.* 93, 193–210. doi:10.1016/j.jseaes.2014.07.013

Xiao, W., and Santosh, M. (2014). The Western Central Asian Orogenic Belt: A Window to Accretionary Orogenesis and Continental Growth. *Gondwana Res.* 25 (4), 1429–1444. doi:10.1016/j.gr.2014.01.008

Xiong, F., Ma, C., Jiang, H. A., and Zhang, H. (2016). Geochronology and Petrogenesis of Triassic High-K calc-alkaline Granodiorites in the East Kunlun Orogen, West China: Juvenile Lower Crustal Melting During Post-Collisional Extension. *J. Earth Sci.* 27 (3), 474–490. doi:10.1007/s12583-016-0674-6

Xiong, F., Ma, C., Chen, B., Ducea, M. N., Hou, M., and Ni, S. (2019). Intermediate-Mafic Dikes in the East Kunlun Orogen, Northern Tibetan Plateau: A Window into Paleo-Arc Magma Feeding System. *Lithos* 340-341, 152–165. doi:10.1016/j.lithos.2019.05.012

Xiong, F., Ma, C., Wu, L., Jiang, H. A., and Liu, B. (2015). Geochemistry, Zircon U-Pb Ages and Sr-Nd-Hf Isotopes of an Ordovician Appinitic Pluton in the East Kunlun Orogen: New Evidence for Proto-Tethyan Subduction. *J. Asian Earth Sci.* 111, 681–697. doi:10.1016/j.jseaes.2015.05.025

Xiong, F., Ma, C., Zhang, J., Liu, B., and Jiang, H. A. (2014). Reworking of Old Continental Lithosphere: An Important Crustal Evolution Mechanism in Orogenic Belts, as Evidenced by Triassic I-type Granitoids in the East Kunlun Orogen, Northern Tibetan Plateau. *J. Geol. Soc.* 171 (6), 847–863. doi:10.1144/jgs2013-038

Xiong, F.-H., Ma, C.-Q., Zhang, J.-Y., and Liu, B. (2012). The Origin of Mafic Microgranular Enclaves and Their Host Granodiorites from East Kunlun, Northern Qinghai-Tibet Plateau: Implications for Magma Mixing during Subduction of Paleo-Tethyan Lithosphere. *Miner. Petrol.* 104, 211–224. doi:10.1007/s00710-011-0187-1

Xiong, F. H., Ma, C. Q., Zhang, J. Y., and Liu, B. (2011). LA-ICP-MS Zircon U-Pb Dating, Elements and Sr-Nd-Hf Isotope Geochemistry of the Early Mesozoic Mafic Dyke Swarms in Eastern Kunlun Orogenic Belt. *Acta Petrol. Sin.* 27, 3350–3364.

Xu, J.-F., Shinjo, R., Defant, M. J., Wang, Q., and Rapp, R. P. (2002). Origin of Mesozoic Adakitic Intrusive Rocks in the Ningzhen Area of East China: Partial Melting of Delaminated Lower Continental Crust. *Geol* 30 (12), 1111–1114. doi:10.1130/0091-7613(2002)030<1111:oomair>2.0.co;2

Yang, J. S., Robinson, P. T., Jiang, C. F., and Xu, Z. Q. (1996). Ophiolites of the Kunlun Mountains, China and Their Tectonic Implications. *Tectonophysics* 258 (1-4), 215–231. doi:10.1016/0040-1951(95)00199-9

Yin, S., Ma, C., and Xu, J. (2021). Recycling of K-Feldspar Antecrysts in the Baishiya Porphyritic Granodiorite, East Kunlun Orogenic Belt, Northern Tibet Plateau: Implications for Magma Differentiation in a Crystal Mush Reservoir. *Lithos* 402-403, 105622. doi:10.1016/j.lithos.2020.105622

Yu, M., Dick, J. M., Feng, C., Li, B., and Wang, H. (2020). The Tectonic Evolution of the East Kunlun Orogen, Northern Tibetan Plateau: A Critical Review with an Integrated Geodynamic Model. *J. Asian Earth Sci.* 191, 104168. doi:10.1016/j.jseaes.2019.104168

Yu, M., Feng, C. Y., Santosh, M., Mao, J. W., Zhu, Y. F., Zhao, Y. M., et al. (2017). The Qiman Tagh Orogen as a Window to the Crustal Evolution in Northern Qinghai-Tibet Plateau. *Earth-Science Rev.* 167, 103–123. doi:10.1016/j.earscirev.2017.02.008

Yu, S., Li, S., Zhang, J., Sun, D., Peng, Y., and Li, Y. (2018). Linking High-Pressure Mafic Granulite, TTG-like (Tonalitic-trondhjemitic) Leucosome and Pluton, and Crustal Growth during continental Collision. *GSA Bull.* 131 (3-4), 572–586. doi:10.1130/B31822.1

Yu, S., Zhang, J., Li, S., Santosh, M., Li, Y., Liu, Y., et al. (2019). TTG-Adakitic-Like (Tonalitic-Trondhjemitic) Magmas Resulting from Partial Melting of Metagabbro under High-Pressure Condition during Continental Collision in the North Qaidam UHP Terrane, Western China. *Tectonics* 38 (3), 791–822. doi:10.1029/2018TC005259

Yuan, C., Sun, M., Xiao, W., Wilde, S., Li, X., Liu, X., et al. (2009). Garnet-Bearing Tonalitic Porphyry from East Kunlun, Northeast Tibetan Plateau: Implications for Adakite and Magmas from the Mash Zone. *Int. J. Earth Sci. (Geol Rundsch)* 98 (6), 1489–1510. doi:10.1007/s00531-008-0335-y

Yuan, H. L., Gao, S., Dai, M. N., Zong, C. L., Günther, D., Fontaine, G. H., et al. (2008). Simultaneous Determinations of U-Pb Age, Hf Isotopes and Trace Element Compositions of Zircon by Excimer Laser-Ablation Quadrupole and Multiple-Collector Icp-Ms. *Chem. Geol.* 247 (1-2), 100–118. doi:10.1016/j.chemgeo.2007.10.003

Zhang, J., Ma, C., Li, J., and Pan, Y. (2017). A Possible Genetic Relationship between Orogenic Gold Mineralization and Post-Collisional Magmatism in the Eastern Kunlun Orogen, Western China. *Ore Geology. Rev.* 81, 342–357. doi:10.1016/j.oregeorev.2016.11.003

Zhang, J., Yu, M., Wang, H., Li, B., Feng, C., Dick, J. M., et al. (2021). Geodynamic Setting and Cu-Ni Potential of Late Permian Xiwanggou Mafic-Ultramafic Rocks, East Kunlun Orogenic Belt, Nw China. *Front. Earth Sci.* 9. doi:10.3389/feart.2021.666967

Zheng, S., An, Y., Lai, C., Wang, H., and Li, Y. (2021). Genesis of High-Mg Adakites in the Southeastern Margin of North China Craton: Geochemical and U-Pb Geochronological Perspectives. *Front. Earth Sci.* 9. doi:10.3389/feart.2021.731233

Zhong, S., Li, S., Feng, C., Liu, Y., Santosh, M., He, S., et al. (2021). Porphyry Copper and Skarn Fertility of the Northern Qinghai-Tibet Plateau Collisional Granitoids. *Earth-Science Rev.* 214, 103524. doi:10.1016/j.earscirev.2021.103524

Conflict of Interest: The authors declare that the research was conducted in the absence of any commercial or financial relationships that could be construed as a potential conflict of interest.